IMPLEMENTATION OF TOMOSYNTHESIS IN DENTAL X-RAY IMAGING

by

Arda Varılsüha

B.Sc., Electronics Engineering, İstanbul Technical University , 2010

Submitted to the Institute of Biomedical Engineering
in partial fulfillment of the requirements
for the degree of
Master of Science
in
Biomedical Engineering

Boğaziçi University
2012

Acknowledgements

It is a pleasure to thank the many people who made this thesis possible. It is difficult to overstate my gratitude to my supervisor Prof. Dr. Cengizhan Öztürk. Thanks to him I had chance to observe different aspects of biomedical engineering. He supported me to achieve my goals and provided me with opportunities along the way.

I would like to thank the X-Lab team, especially "my boss" Aytaç Durmaz for his technical, motivational and logistic support in the lab. I also would like to thank to my lab partners, Mustafa Porsuk and Merve Atik for their company and tolerance. I wish them the best of luck.

I thank the other team members of Kandilli, especially Tuğba Gözdamla and Sevim Tekeli for their support and motivation. I hope they will stay as essential members at Kandilli for years to come.

I would like to thank my best friend İslam Tete for all the good times we share for many years. I also like to thank to Cem Sümengen and Bilgin Kızıltaş for their comradery both during and after ITU. I hope that our paths will cross again somewhere and sometime in life.

Finally I would like to thank to my mother and father for all their support from the day I was born. I cannot possibly repay them in any way.

This thesis is dedicated to my grandmother.

Abstract

IMPLEMENTATION OF TOMOSYNTHESIS IN DENTAL X-RAY IMAGING

Digital tomosynthesis is a method of reconstructing any number of tomographic planes, by using a set of limited angle projections, acquired as the X-ray source moves around the object. The quality of the reconstructed planes is affected by structured artifacts, due to blur from planes other than the plane-of-interest. In this project a special multiple projection algorithm along with an out-of-plane blur removal method is implemented to improve the image quality.

In-silico phantom experiments was employed to evaluate the parameters that affect the image quality in tomosynthesis. Different groups were created with varying arc lenghts and projection counts. A blur removal method was implemented during image reconstruction to increase image quality. Image quality was evaluated by both visual assessment and structural similarity analysis. The proposed noise removal algorithm resulted in images with less artifacts.

Preliminary tests of the algorithm were also done in a physical dental phantom. The results showed that the tomosynthesis image reconstruction could be a promising and a low cost method to evaluate digital dental x-rays without excess radiation to the patient.

Keywords: Tomosynthesis, X-ray, Digital imaging, Dental imaging.

Özet

TOMOSENTEZİN DİŞ X-RAY GÖRÜNTÜLERİNE UYGULANMASI

Dijital tomosentez, X ışını kaynağının nesne etrafında oluturduu bir hareketle, sınırlı bir açı diliminde aldığı görüntüleri kullanarak istenen kesitleri oluşturma yöntemidir. Oluşturulan kesitlerin kalitesi, odaklanılan kesitin dışında kalan kesitlerdeki yapıların oluşturduğu bulanıklık sebebi ile etkilenebilir. Bu çalışmada, özel bir çoğul görüntüleme algoritması uyarlamak ve kesit-dışı bulanıklığı giderme metodu, kesitlerin görüntü kalitesini arttırmak için kullanlmtr.

Tomossentezde görüntü kalitesini etkileyen etkenleri değerlendirmek için bilgisayar ortamnda fantom deneyleri yapılmıştır. Farklı açılarda ve projeksiyon sayılarında gruplar oluşturulmuştur. Tomosentez ile oluşturulan kesitlerde hem görsel olarak, hem de yapsal benzerlik analizi kullanılarak görüntü kalitesi değerlendirilmiştir. MPA algoritması ve bunu takiben uygulanan gürültü azaltma algoritması, az gürültülü tomosentez görüntüleri, yüksek işaret-gürültü oranı ve yüksek kontrast sağladığı görülmüştür.

Geliştirilmekte olan bu teknik, gerçek diş fantomu kullanılarak elde edilen bir görüntü setine de uygulanmıştır. Sonuçlar, tomosentez görüntü oluşturmanın, dijital diş röntgen uygulamalar için umut vaadeden, düşük maliyetli ve hastanın düşük radyasyona maruz kaldığı bir yöntem aday olabileceğini göstermiştir.

Anahtar Sözcükler: Tomosentez, X-ışını, Dijital görüntüleme, Diş görüntüleme.

Contents

List of Figures

List of Tables

List of Symbols

S	position of source at zero angle
S'	position of source at angle ω
L	distance from isocenter to anatomic structure
B	source to isocenter distance
D	source to image receptor distance
IA	horizontal plane through isocenter
I_iA_i	acquired image of IA on image receptor
I_hA_h	projection of I_iA_i onto horizontal plane
QP	structure lying at distance L from isocenter
Q_iP_i	acquired image of QP on image receptor
Q_hP_h	projection of Q_iP_i onto the horizontal plane
Q_rP_r	resized image of QP on image formation plane.

List of Abbreviations

MPR	Multiple Projection Reconstruction
DTS	Digital Tomosynthesis
CT	Computed Tomography
SSIM	Structural Similarity Index
MSSIM	Mean Structural Similarity Index

1. Introduction

1.1 Introduction

X-ray imaging is one of the most commonly used techniques in medical imaging. It is based on X-rays which are a kind of electromagnetic radiation. X-rays can pass through human tissue more or less unaffected. Some tissues - especially bones - absorb more radiation than others - soft tissues like muscles and fat-; while air in the mouth, lungs or body cavities has almost no effect at all on the radiation. As a result, a film placed on the one side of the patient that is facing an X-ray source on the other side, will capture an image of the bones and other tissue in proportion to the absorption coefficients of different tissues.

Currently the films in X-ray imaging are replaced by digital sensors or a phosphor imaging plates, These can be used repetitively unlike the disposable film. Moreover, they give images in digital form. A digital image has many advantages over conventional film: it is easier to distribute and process the images (contrast, brightness, equalization, sharpening etc.).

In digital intra-oral dental imaging, the sensor is placed inside the patient's mouth. X-rays are irradiated outside the mouth and the structure of the teeth and other tissues are imaged on the sensor, which captures the x-rays.

Tomosynthesis is a technique that can provide images at different angles. These images can be used separately or can be used to reconstruct an image that has depth information. Since it uses only a limited angle image set, the patient is exposed to less radiation than CT imaging. It could potentially give the information needed faster and in a less harmful way.

The purpose of this thesis work is to test the initial feasibility of this tomosynthesis technique in intra-oral dental imaging and to understand if it has the potential to give the dentist acceptable quality images of the dental structures. This information could speed up the diagnosis phase, prevent any possible malpractice caused by standard limited 2D measurements and decrease the unnecessary radiation that is caused by repeated CT scans.

1.2 Literature Review

1.2.1 History and Technology of X-Ray Imaging

X-rays (or Roentgen rays) were found by a German physics professor, Wilhelm Conrad Röntgen, on November 8, 1895. Prof. Röntgen, Director of the Physical Institute of the University of Würzburg, was interested in work of Hertz and Lenard and many others on electrical discharges in vacuum tubes. He set up his own apparatus and followed and repeated the work of predecessors, namely the work done by Hertz and Lenard [1]. They had been carrying out experiments with the Hittorf-Crookes tube. This tube has a partially evacuated glass envelope with two electrodes separated by a distance of a few centimeters. When a potential difference of few thousand volts is connected between the electrodes; the partially ionized, rarified gas in the tube is accelerated by the electric field. Due to the high voltage, the ions accelerate and hit the cathode (negative electrode) with such energy, that they manage to release electrons from the surface of the cathode [1, 2].

As electrically charged particles, the electrons are accelerated in the electric field away from the cathode and towards the anode (positive electrode). Should the voltage between the electrodes be huge enough, some of the accelerated electrons might overshoot, or go through the anode and strike the glass wall of the tube, emitting x-rays, though this wasn't known at the time.

X-rays are part of the same electromagnetic radiation as visible light and radio waves, ranging from frequencies of $30x10^{15}$ Hz to $30x10^{18}$ Hz. In the spectrum of the electromagnetic radiation they are between lower frequency ultraviolet and higher frequency gamma-rays. The frequencies of x-rays and gamma-rays overlap and the only difference between the two is the method the rays were generated. Gamma-rays are formed by transitions within atomic nuclei or matter-antimatter annihilation, while x-rays are generated when high-speed electrons are decelerated in matter [3].

Electrons decelerating in matter was what happened in the Röntgen's tube when the overshot electrons hit the glass, causing x-rays were to emit. While carrying out his experiments with cathode rays, Röntgen made a discovery of fluorescence of a paper screen covered with barium platinocyanide crystals. The paper screens were used to detect whether there were cathode rays present or not. To use these papers, a special kind of tube with aluminum window was needed to pass the cathode rays outside the tube. This time, however, there was fluorescence even when working with a glass tube which shouldn't pass cathode rays. Röntgen realized he had found a new kind of radiation, and, unaware of the true nature of the radiation, called it the "x-ray" [2].

Röntgen became more experienced with these rays and made a publication on them. The medical potential was understood soon and the first skeletal radiographs of a living hand were taken less than two months after the discovery of the radiation [4]. .

A modern dental x-ray tube is still similar to the tube Röntgen used on his experiments (Figure 1.1). Electrons are emitted from a lament that is heated by an electric current. Voltage difference between cathode and anode forces the electrons to travel to the anode, where a tungsten target is located. X-rays are emitted when electrons decelerate in this target.

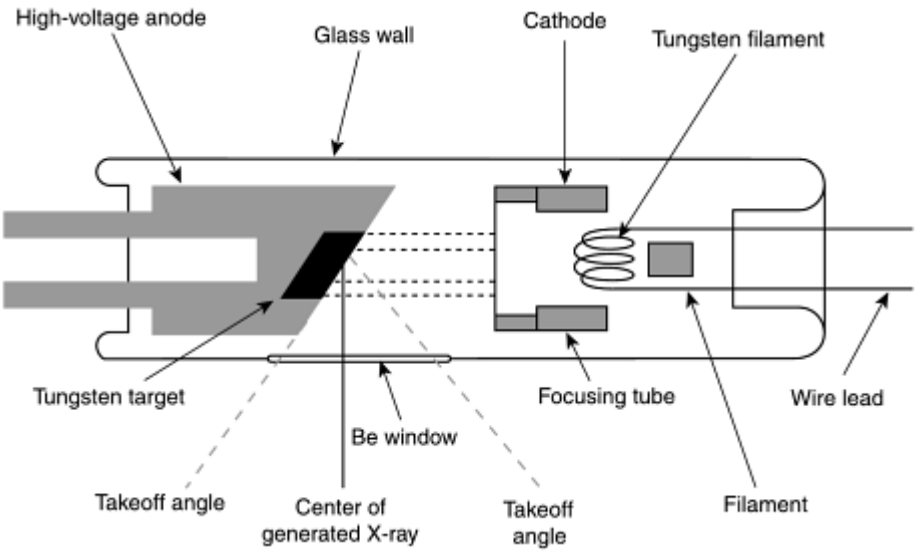

Figure 1.1 A Modern X-Ray Tube[5]

X-ray images were first recorded by films. One of the properties of the film is that, the more radiation there is, the darker the image becomes. Therefore soft tissues in x-ray images show darker than bones, as more radiation passes through them. X-ray images are still shown in the same manner (as negative images), even if they are recorded by other recording media [5].

1.2.2 Modern Dental Imaging

Modern dental radiography is divided into three fields. Intra-oral radiography was the first dental imaging method. In intra-oral radiography, a certain recording medium is placed inside the patient's mouth (hence the name intra-oral).

X-ray tube - the source of x-ray - is located outside the head so that the radiation passes through the object and hits the recording medium. Recording medium might be either (now almost obsolete) film or in more modern devices either a reusable phosphor imaging plate or an image sensor. Recording medium

of various sizes are used. The size of the medium is a trade-off between the area of the imaging, and the comfort of the patient due to the limited space in the mouth [6].

There are several views used in intra-oral radiography. They are used for different needs but are fundamentally similar. Periapical view means the recording medium is located in the mouth so that it records an image of whole tooth including the crown and root (Figure 1.2). This view might be used to determine the need for endodontic therapy, or to look for aching tooth [6].

Figure 1.2 Periapical View [5]

In bite-wing view the recording medium is placed so that it records the image of the crowns of the teeth, which are usually the region of interest (Figure 1.3). One exposure records evenly the crowns of both maxillary (upper) and mandibular (bottom) teeth [6].

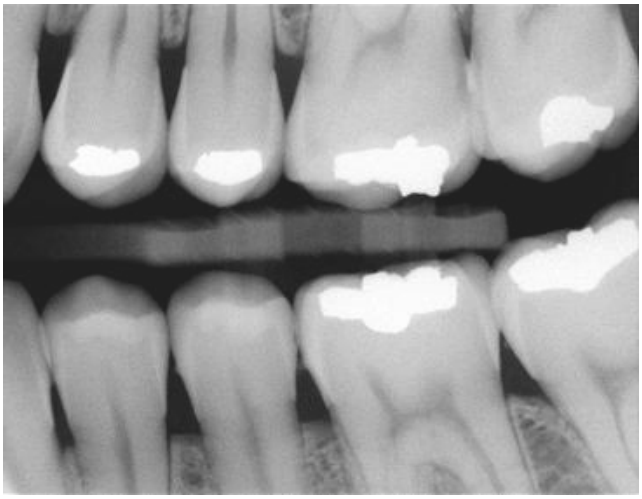

Figure 1.3 Bitewing View [5]

Lastly, occlusal view is used to get an image either from all maxillary or all mandibular teeth (Figure 1.4). The recording medium is placed between patient's upper and lower teeth. For upper teeth the x-ray tube is located above the nose, and for bottom teeth it is located below the jaw. The recording medium for occlusal view is larger than the one used for periapical or bite-wing views [6].

Figure 1.4 Occlusal View [5]

In tomography imaging the recording medium is located outside the patients mouth and is hence in the group of extra-oral imaging methods in dental imaging. The x-ray tube and recording medium are at the opposite sides of the object to be scanned. The tube and film both rotate - or move otherwise, e.g. on linear or spiral path - in opposite directions around a fixed point, which determines the location of the imaging layer [7].

Imaging layer is a predetermined plane which gets recorded sharply in the tomography. In intra-oral imaging, all the matter-not only the desired one-between the tube and film ends up to the image (Figure 1.5). For tomography imaging the same holds, however, because of the movement of both x-ray tube

and recording medium, only one layer is scanned sharply. Tissue far from this desired layer will leave a widely spread, faint haze to the image, which will be seen as noise in the final image [7].

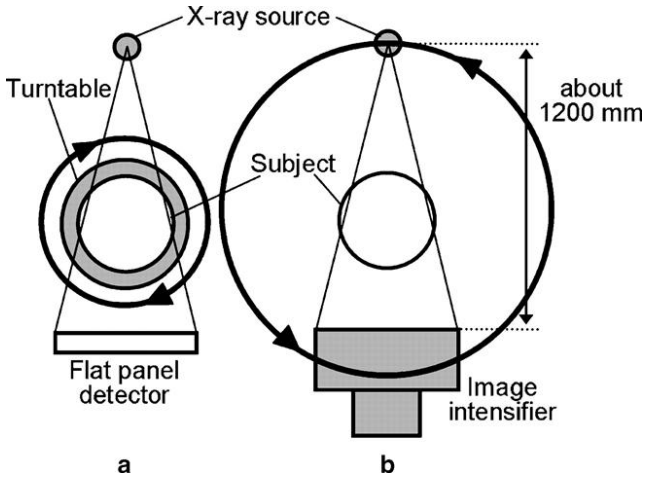

Figure 1.5 Sketch of the movement the x-ray tube and recording medium participate in tomography imaging. Tube and medium (denoted by f) move to opposite directions around a center point which will determine the location of the imaging layer (s), the plane of tissue to be shown sharp in final image [5].

After few stages of development, an orthopantomography was introduced where the focus point follows the teeth during the scan with rather narrow beam (Figure 1.6). Narrowed beam means only a small vertical slice of the film will be exposed at the time, thus recording an image of the teeth at the current focus point only. As the focus point slowly moves, the film slides in the sledge and the imaging of the new focus point gets recorded to the newly revealed part of the film [6].

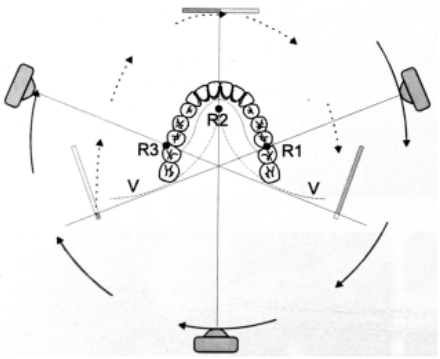

Figure 1.6 A sketch of the rotation of the x-ray tube and the film casing in the orthopantomography device. The focus point follows the presumed curve of human teeth thus recording a sharp image of all teeth [6].

After the whole round, a panoramic image of the teeth is recorded. Other that teeth, both chin and sinus are also visible in the image (Figure 1.7).

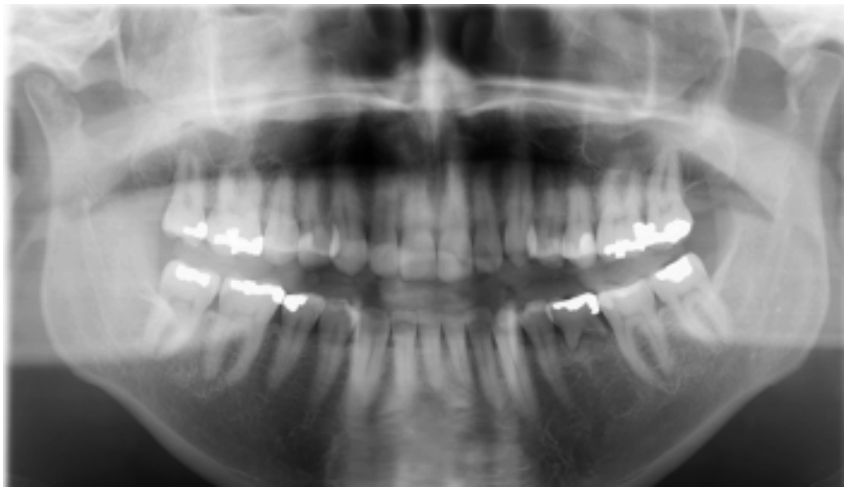

Figure 1.7 An example of panoramic image taken with digital orthopantomography device. [6].

On more modern, digital orthopantomography device, the film is replaced by a digital sensor. The film size on non-digital devices varies between different apparatus but might be e.g 15-30 cm. Digital sensor, however, might be significantly smaller. Like in the case of film device, the beam is narrow and only a small vertical slice of teeth and skull is exposed at the time. Recorded data is read from the sensor at certain intervals and the sensor is reset to zero. This is equivalent to sliding a film in a sledge so that the beam next hits an unexposed

part of the recording medium, and there is no need to slide the sensor as is in the case of a film device. Panoramic image of teeth and skull is composed of these narrow slices [6].

The result is either a series of slices orthogonal to one axis or true three-dimensional image of the scanned volume. From the 3D-data collected by CT device, it is also possible to generate images similar to orthopantomography and intra-oral imaging.

1.2.3 Digital Tomosynthesis

Some limitations of the two dimensional radiography were overcome after the development in computed tomography (CT) in 1970 [8]. This three-dimensional (3D) imaging technique made it possible to localize the depth information, provided enhanced visibility and contrast by focusing the exact plane of interest of a structure. Tomosynthesis imaging principle is basically, as seen in Figure 1.8, to acquire the image plane of interest by rotating the x-ray tube and the detector around the patient. The pivot point of this rotational motion is the focused image plane of interest. Thats why other planes that are left out of focus plane are obtained blurry. The blurring caused by these other planes veils detail in the plane of interest and limits the contrast enhancement of the slices [9].

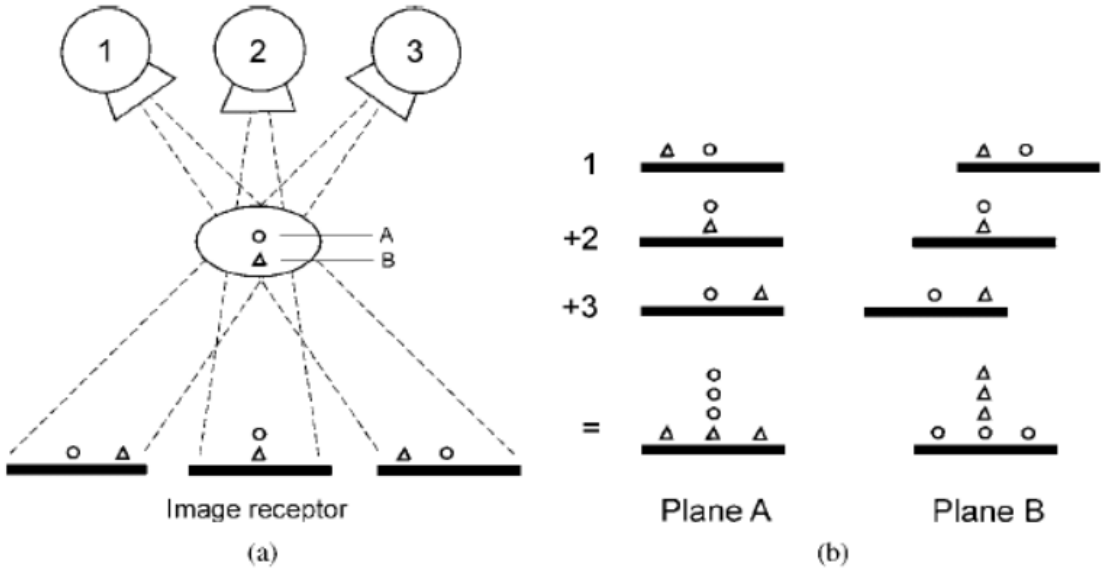

Figure 1.8 In Figure 1.8(a) three locations of the x-ray tube are depicted, above a circle shaped object in one plane and a triangle shaped object in another plane. The relative projected locations of the circle and triangle are shown in the same figure. In Figure 1.8(b), three resulting projection images are shifted and added in order to bring either the circles or triangles into coincidence, causing focusing of that structure [10].

3D orientation of anatomy could be understood by distinguishing the image plane-of-interest from the objects in other planes. While this image improvement proved an advantage of the computerized tomography; excessive radiation dose and time consumption to acquire every single one of the slices to reconstruct the volumetric image caused problems. Furthermore, to overcome the blurring problem, intricate mechanical motions (e.g. linear, circular and even hypo-cyclodial motions) to calibrate the pivot location were required. Other restriction was that collecting image projections over 360° was not always possible. In C-arm systems this motion was limited to around 200° .

To overcome the aforementioned restrictions of 3D imaging of conventional tomographic imaging; limited angle reconstruction methods were introduced such as digital tomosynthesis [11, 12].

Tomosynthesis is a method for limited angle CT, a 3D imaging technique which provides reconstruction of an arbitrary number of tomographic planes with

reduced cost and radiation over a limited angle of view [13, 14]. Apart from the reconstruction methods, the mechanical system design is not very different from CT. X-ray tube moves along a limited angle arc enabling multiple 2D projections of the target object at these different angles. Generally it is performed using 10 to 25 2D-projections over an arc of 15° to 50° angles. Algorithms like shift-and-add allow reconstructing the volumetric image from these limited angle projections. Combining the information contained in each planes at different angles enhances the image plane of interest. The image information increases gradually by adding the information in different image projections. So that the structure in the focused image plane of interest can be seen greater detail with reduced dose (Figure 1.8)[10].

Tomosynthesis theory was first introduced in as early as 1972 by Grant [15]. Initially it was based on the work of conventional tomography. Despite the advantages mentioned, the practical implementation was possible only after the development of flat-panel detectors which have large area, high frame capture rate, high contrast, low noise and fast read times, which enabled large number of low dose projections to be acquired rapidly. Further research and clinical potential is improved dramatically after the various digital detectors come to stage [16, 17].

1.2.4 Dental Applications

Tomosynthesis could be a promising technique in dental imaging since dentistry requires open and mobile systems. Moreover in dentistry the attenuation path of the X-ray beam during tomosynthesis is more favorable than in standard body CT. An intra-oral projection geometry was modeled in an experimental set-up by Lauritsch, G et al. [18]. The components of a specific intra-oral X-ray system were used with a 60kV X-ray focus (1.5mm Al filter) and a CCD-detector having a pixel size of 5μm in each direction and a 12-bit gray level resolution. A three rooted molar tooth in a piece of a maxilla surrounded by a filling material

to model soft tissue was exposed 0.08s at an anode current of 7mA for each radiograph (projection image). To form a set of projection images 24 radiographs were taken at a circular scanning geometry and a tomographic angle α=12°. In Figure 1.9 we see the image results reconstructed by simple back projection (or simple superposition) [18].

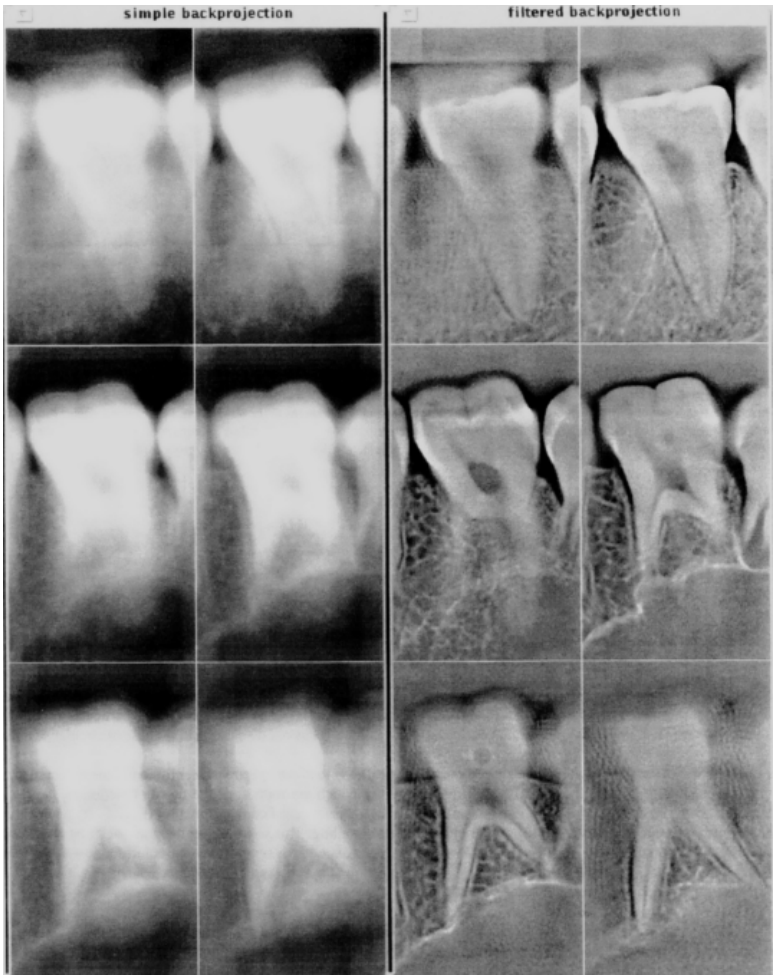

Figure 1.9 Tomosynthetic reconstructed images of a specimen of a three-rooted molar tooth of the maxilla. Left frame: set of six image slices reconstructed by simple back projection. Right frame: set of six image slices reconstructed by filtered back-projection. In both cases the image slices are identically positioned. The distance between subsequent slices is 2.5mm. The slice images are spatially ordered 1mm left to right, and from top to bottom [18].

1.3 Motivation and Objectives

The purpose of this thesis is to implement an algorithm to create tomosynthesis image for limited angle dental X-ray projections. For this purpose, initially

a set of simulated projection images in the gantry arc from -45° to 45° (every 10°) is used. These projections were reconstructed with the MPR algorithm written in MATLAB. Next, a noise removal step was implemented to further increase the image contrast. Image quality was assessed by evaluation of the reconstructed planes in terms of both visual assessment and SSIM index.

Once the preliminary tests are completed another digital simulation phantom is created in MATLAB for further evaluation. Initially projection images in the gantry arc from -20° to +20° for every 2° angle step were created. Several different image groups are created within these projections, varying the acquisition arc angle and the step angle. These projections were reconstructed with the MPR algorithm. Image quality between groups was assessed by evaluation of the reconstructed planes in terms of both visual assessment and SSIM index.

Lastly, a preliminary clinical data set was created from a dental phantom using a Siemens CT system. Raw data from this system was used in the implemented algorithm with different arc angle and step angle combinations. Different image focus planes both from the tomographically reconstructed data and tomosynthesized data were compared.

Specific objectives of this project were:

1. Write the necessary software code to implement the tomosynthesis reconstruction methodology for the case of a movable detector in a circular configuration.

2. Write the necessary software code to implement the tomosynthesis blur removal methodology for a circular configuration, in order to remove the blur artifacts produced by structures positioned outside the reconstructed plane.

3. Evaluate the feasibility of this technique in real dental image sets.

1.4 Thesis Outline

This thesis is comprised of four main sections.

In the first section, the subject is introduced. History and technology of X-Ray imaging is described. Dental imaging is explained in further detail as a particular application of X-Ray imaging. Several methods are explained in dental imaging. Digital tomosynthesis is analyzed as a 3D imaging method and the studies of dental applications of this method is discussed. Lastly the motivation and the objectives of the study are stated.

In the second section, materials and methods used in this thesis are described. The theories of the methods and algorithms, (namely the MPR algorithm, removal of out-of-plane structures) and Structural Similarity Index (SSIM) are explained. Furthermore the data sets (software simulation and dental phantom data sets) used in these methods are depicted.

In the third section, the results are presented for both the software simulation data set and the dental phantom data set.

In the fourth section these results are presented and discussed in detail.

In the fifth and sixth sections the conclusion that arises from these results are given and possible future works are listed to further develop this method.

2. Materials and Methods

2.1 The Multiple Projection Algorithm

The image reconstruction algorithm in this thesis, is developed based on the work of Kolitsi [19]. It was developed as a multiple projection digital tomosynthesis method to be used in isocentric fluoroscopy units. More precisely, it is capable of producing digital tomosynthetic images, of anatomical planes of user selected orientation and distance from the isocenter. This reconstruction is made possible by shifting the locations of pixels in each projected image so that they are aligned with an abstract image formation plane. In other words this plane can be considered as a flat image receptor appropriately coupled in motion to the x-ray source. In this way an integration of the signal at the receptor over an acquisition arc, leads to the reconstruction of the tomographic image of the selected plane in the scanned phantom. The reconstruction process is divided into discrete transformation for group of pixels and not for individual pixels. In this way the method becomes very efficient concerning the computation time compared to other methods. At the end, the shifted images from all projections are summed to produce the final reconstructed image at the desired depth and inclination. The image reconstruction geometry is shown in Figure 2.1.

In this figure the subscript i denotes the column number in the acquired image matrix. The subscript r denotes the position on the reconstructed image matrix to which the corresponding matrix column i is moved.

S= position of source at zero angle

S'= position of source at angle ω

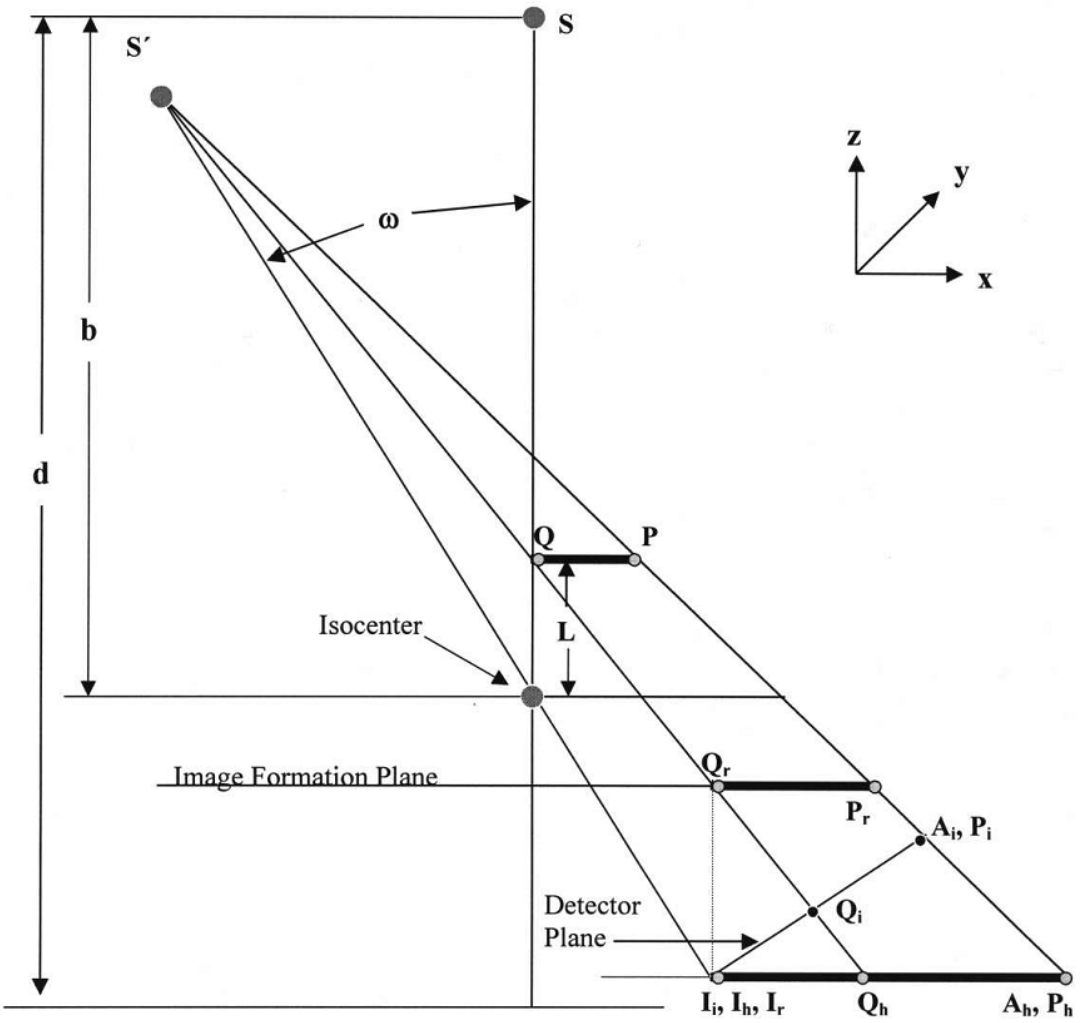

Figure 2.1 Scheme representation of the acquisition and reconstruction of tomosynthesis data [11].

L= distance from isocenter to anatomic structure

B= source to isocenter distance

D= source to image receptor distance

IA= horizontal plane through isocenter

I_iA_i= acquired image of IA on image receptor

I_hA_h= projection of I_iA_i onto horizontal plane passing through the intersection of the beams central axis and the detector plane. This is the image formation plane for an anatomic structure positioned at isocenter. Adding these projections over all sampling angles will yield the reconstructed image of IA.

QP= structure lying on a horizontal plane at a distance L from isocenter

Q_iP_i = acquired image of QP on image receptor

Q_hP_h= projection of Q_iP_i onto the horizontal plane passing through the intersection of the beams central axis and the detector plane

Q_rP_r= size modified, focused image of QP on its image formation plane.

Addition of these projections over all sampling angles will yield the reconstructed image of QP. For horizontal planes lying away from isocenter, the image formation plane is a horizontal plane suspended from point Q_r. During rotation and acquisition, the distance $I_iQ_r = Ld/b$ remains constant for a given L. The loci of the suspension point Q_r therefore lies on a circle of radius$(d - b)$, but with the center displaced by an amount equal to I_iQ_r from isocenter. The reconstruction of a horizontal plane uses the following equations for column shifts

in the matrix:

$$h = \frac{id}{d.\cos\omega - i.\sin\omega} \tag{2.1}$$

$$r = (h - \frac{(Ld.\sin\omega)}{(b.\cos\omega - L)}) * (1 - \frac{L}{b.\cos\omega}) \tag{2.2}$$

Finally, when planes outside the isocenter are reconstructed, the tomosynthesized image must be appropriately magnified in the direction perpendicular to the plane of rotation by shifting rows by the factor$(bL)/b$. For eliminating the unwanted vertical bands, the filtration starts with the image formation plane pixel location and selects pixel values from the projection image data for weighting and summation in the target image formation plane pixel, thus preventing the appearance of gaps in the image formation plane. In order to remove unwanted structured noise from the plane of interest, several algorithms could be employed

2.2 Selective Removal of out of Plane Structures

Digital tomosynthesis (DTS) is a method of limited angle reconstruction of tomographic images, produced at variable heights, on the basis of a set of angular projections [20]. A limitation in the size of sampling arc arises from the restricted movement of the tube-detector assembly. Limited angle DTS reconstruction allows for the recovery of a limited space in the Fourier domain, therefore DTS tomograms are invariably affected by tomographic noise, i.e. blurred images of structural detail, lying outside the plane of interest, and superimposed over the focus plane. The central slice theorem in 3D, states that the Fourier transform of

a projection corresponds to a slice of the Fourier transform of the object. That means that one parallel beam projection is equivalent in Fourier space to a plane trough the origin, perpendicular to the rays emitted from the source point. In the case of the isocentric rotational DTS, projection images are acquired on arc of ś20° with respect to the vertical. The information acquired for the limited arc used for DTS, leaves an incomplete region in the Fourier space as it can be seen in Figure 2.2.

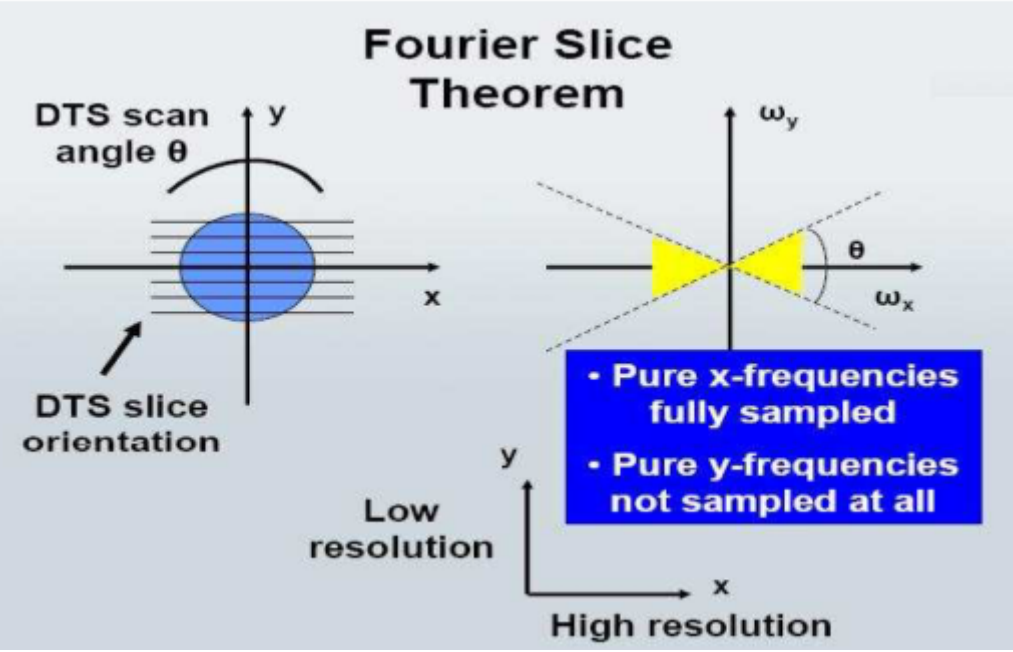

Figure 2.2 Schematic representation of the Fourier Slice Theorem [20]

The empty space causes a low resolution in the y-direction of the reconstructed volume, which means that in this direction it will not be possible to measure the length of a structure. The bigger the angle of the sampling arc, the smaller this empty area will be and the more the artifacts will be reduced. When the angle becomes 180°, the Fourier space will be completely filled and the reconstructed image will be free from artifacts.

One of the methods for removal of blurred images of out-of-focus planes from the plane of interest has been studied by previously [9, 20]. The method

involves the reconstruction of the blur originating in user-selected "noisy" planes as it appears on the plane of interest. This is achieved by projecting the reconstructed images of the selected plane on the image formation plane for all viewing angles, and subsequently, synthesizing its blurred image on the plane of interest. Reproduction of the noise is performed using the tomosynthesis algorithm itself, thus the technique can be modified to suit any reconstruction algorithm. In this thesis, this technique was implemented on the MPR algorithm. The operations performed by the algorithm, once the acquired image has been projected onto the image formation plane, can be summarized in the expression

$$r = (h - \delta h).m, \tag{2.3}$$

where h and r are the positions of column i in the projected and the reconstructed image matrix (Figure 2.3), respectively.

Now, let $I_N(r,p)$ be the tomosynthesized image matrix of the plane that has been selected for removal. This plane is also imaged in I_0, blurred and attenuated; the objective is then to reconstruct the image of this plane as it appears in I_0 by the tomosynthetic process.

For each one of the viewing angles involved in the reconstruction, matrix $I_N(r,p)$ is first projected back on to the plane of image formation. This step involves a reversal of the operations described by expression 2.3:

$$h_N = r_N/m_N + \delta h_N. \tag{2.4}$$

These projections are subsequently used to tomosynthesize an image on

plane I_0. Thus, they are handled by the algorithm in the same manner as the acquired images, once they have been projected onto the image formation plane. That is, they are first translated by δh_0 and then magnified by m_0:

$$r_{N,0} = (h_N - \delta h_0)m_0. \tag{2.5}$$

The resulting matrices are summed over all viewing angles to give the image plane I_N as it resides on I_N, appropriately blurred and attenuated. The mask image is formed by averaging noise images from all selected planes. The sequence of the operations executed by the noise removal algorithm are summarized Figure 2.3.

2.3 Structural Similarity Index

Structural Similarity Index (SSIM) is a method for evaluating image quality. This measure attempts to mimic the ability of human visual perception to extract structural information from a scene. SSIM assesses image quality based upon the degradation of structural information [21]. The basic equation for SSIM is:

$$SSIM(x,y) = \frac{(2\mu_x\mu_y + C_1)(2\sigma_{xy} + C_2)}{(\mu^2{}_x + \mu^2{}_y + C_1)(\sigma^2{}_x + \sigma^2{}_y + C_2)} \tag{2.6}$$

where μ_x,$\mu_y$are the means, σ_x,σ_y the standard deviations and σ_{xy} the correlation of the local patterns. The two constants C_1 , $C_2 << 1$ are used to avoid numerical instability. To acquire a single overall quality measure of the entire image from the MxN SSIM map, the mean index (MSSIM)

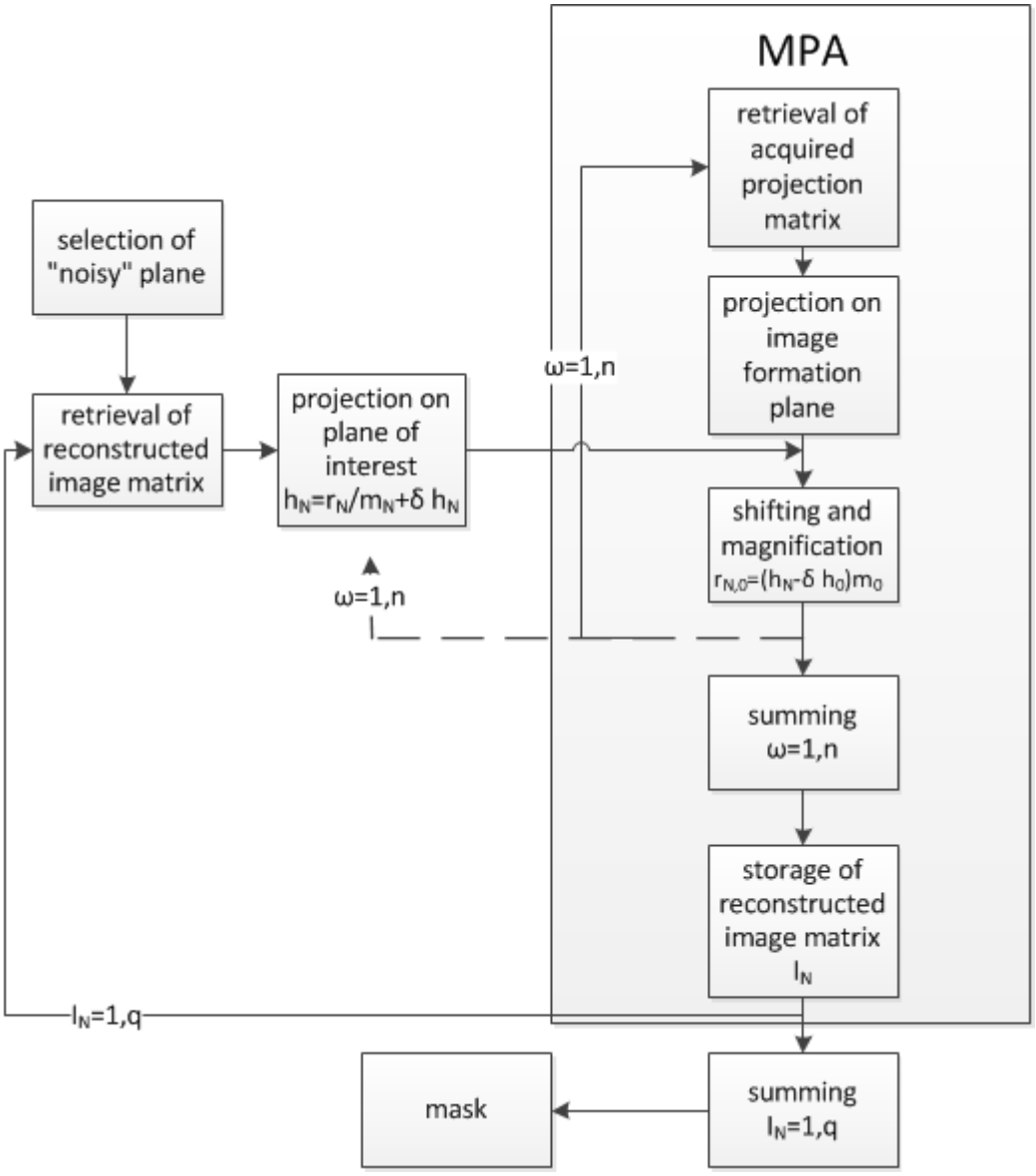

Figure 2.3 MPA and Noise Removal Flowchart

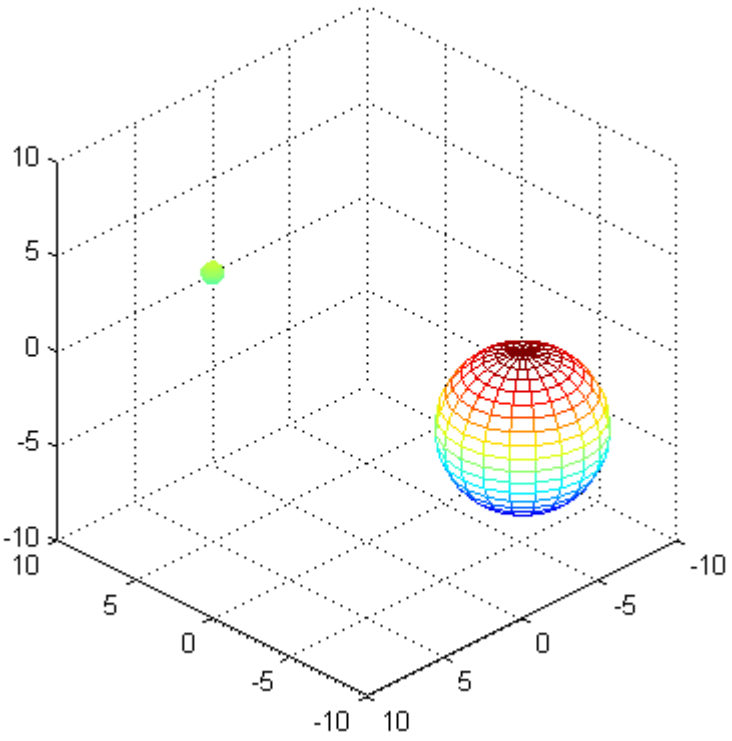

Figure 2.4 3D representation of the simulation data set-I

$$MSSIM(X,Y) = \frac{1}{MN}\sum_{i=1}^{MN} SSIM(x_i, y_i) \tag{2.7}$$

between the two images is calculated. The MSSIM range is [0,1] . "1" meaning the perfect correlation. This thesis uses Wangs MATLAB implementation to assess SSIM.

2.4 Simulation Data

2.4.1 Simulation Data Set I

Initially, a simulation data set was used to test the algorithm. This data set consisted of projections of two spherical shapes from angles with 10°differences over a ±45° arc. A 3D representation of this data set can be seen in Figure 2.4.

The projections of this data set from different angles can be seen in Figure 2.5. It can be seen that at certain angles (from -15° to 15°) the smaller sphere is covered by the larger sphere thus making it invisible. On the other hand, acquisitions from other angles give the false impression that these spheres are located side by side. Creating a tomosynthetic image by using combined information in all acquisitions, could give us the depth information, understanding the positioning of these two objects.

2.4.2 Simulation Data Set II

In order to test the developed algorithms further another simulation data set was created in MATLAB. The scene consisted of three spherical objects in a 3D space with varying radii (4 cm, 2 cm, 1.5 cm). The centers of the 3 large spheres are located on the Z-axis (-6 cm, 0 cm, 4 cm). 3D view of this data set is in Figure 2.6.

Centers of these four spheres are located on one axis. Additionally a smaller sphere was created inside of the smallest sphere's region to model a small tooth anomaly. Center of the middle sphere is located on the origin of the 3D space. This point is also the pivot point (isocenter) of the projection geometry. The source is aimed towards this point and it is moved on the XY plane around the Z-axis over a circular arc. The projections were collected over an arc for a limited angle of $\pm 20°$ with 2° steps between each projection. The reason for selecting the imaging arc limitations is that it would be realistic in clinical dental image acquisition. These simulated noise-free projections can be seen in Figure 2.7.

It can be seen that at certain angles the smallest sphere is covered by larger spheres in front of it thus making it invisible. Creating a tomosynthetic image at arbitrary planes by using all information contained in all acquisitions,

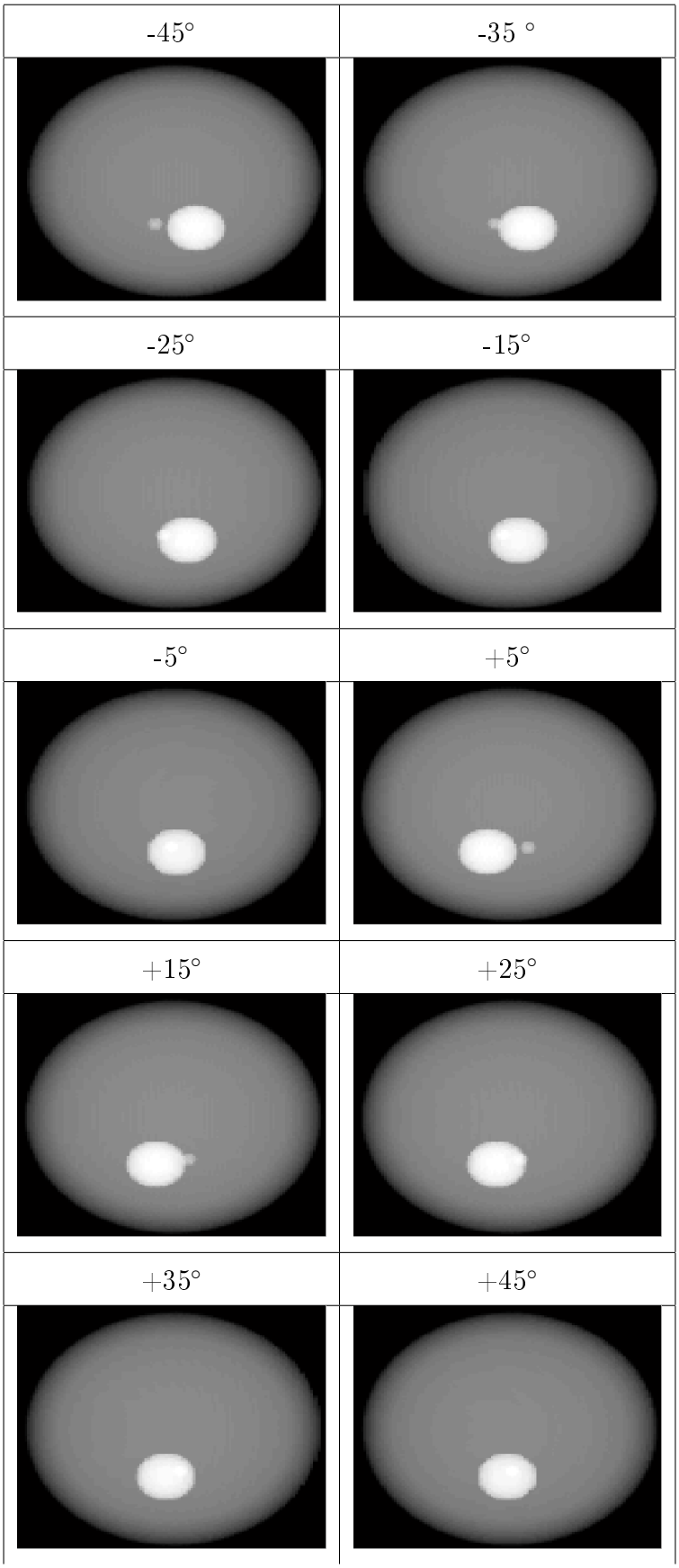

Figure 2.5 Projections from 10 different angles of the simulation data set .

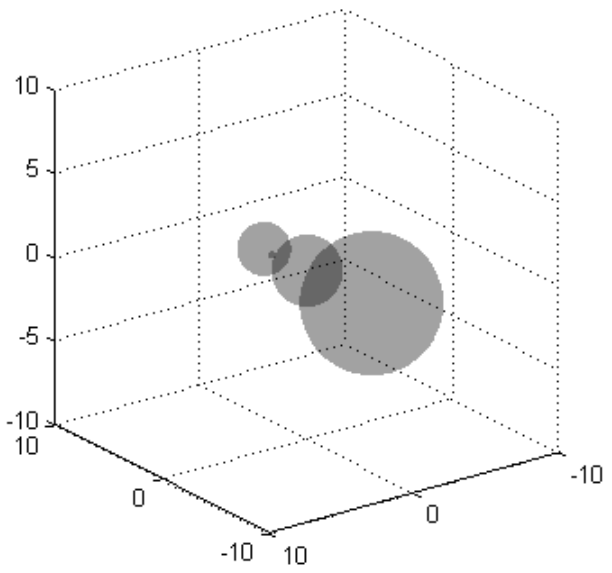

Figure 2.6 3D representation of the simulation data set-II .

creates the necessary contrast and emphasis for the objects exactly in that plane and gives us the depth information to locate the exact positions of the objects.

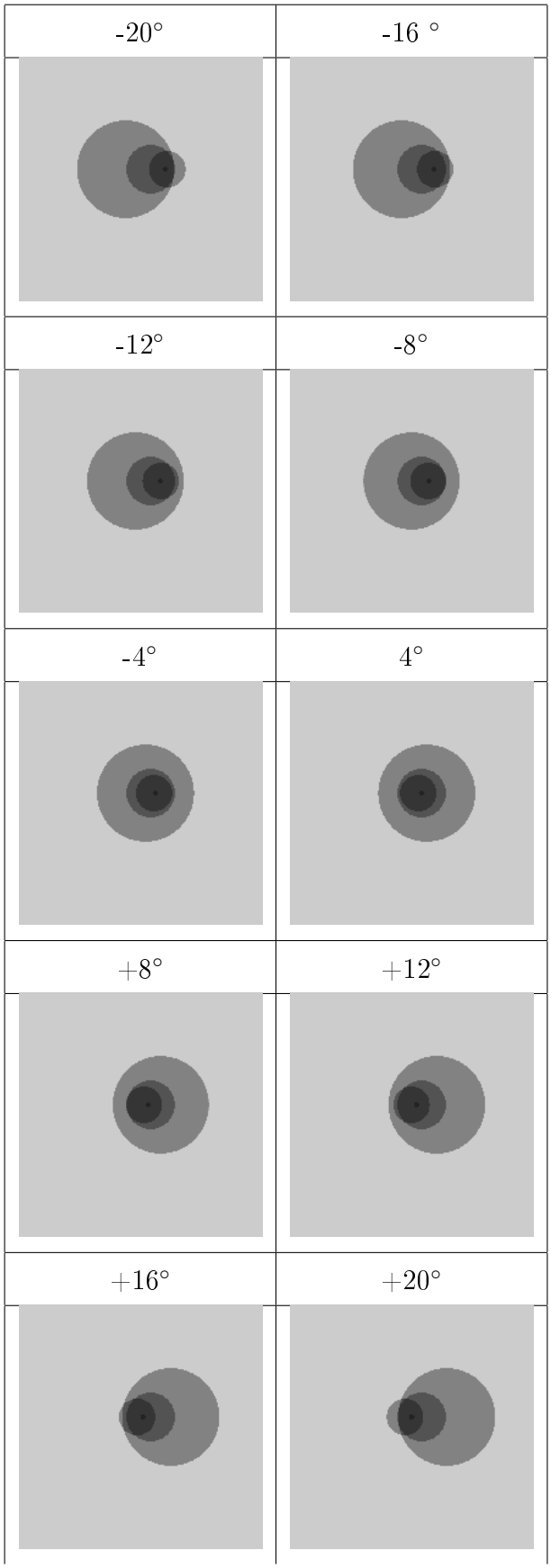

Figure 2.7 Simulation Data Set II

2.5 Phantom Data

In the last part of this study, a more realistic imaging data was obtained from the tomographic images of a dental phantom. The phantom is a Gammex 501A dental phantom. It is consisted of three real molar teeth and one premolar tooth inside the jawbone. A Siemens CT system was used to obtain these projections. A sample of images from the aforementioned data set can be seen in the Figure 2.8 below. The DICOM file created with the system contained source-to-image intensifier, source-to-isocenter distances, acquisition angles and the images at different tags. The images are acquired with an arch of $\pm 200^{\circ}$ with 1.5°intervals. Different photosynthesizing parameters (acquisitions arc, image count) are used to evaluate the different reconstructed image outputs of the algorithm.

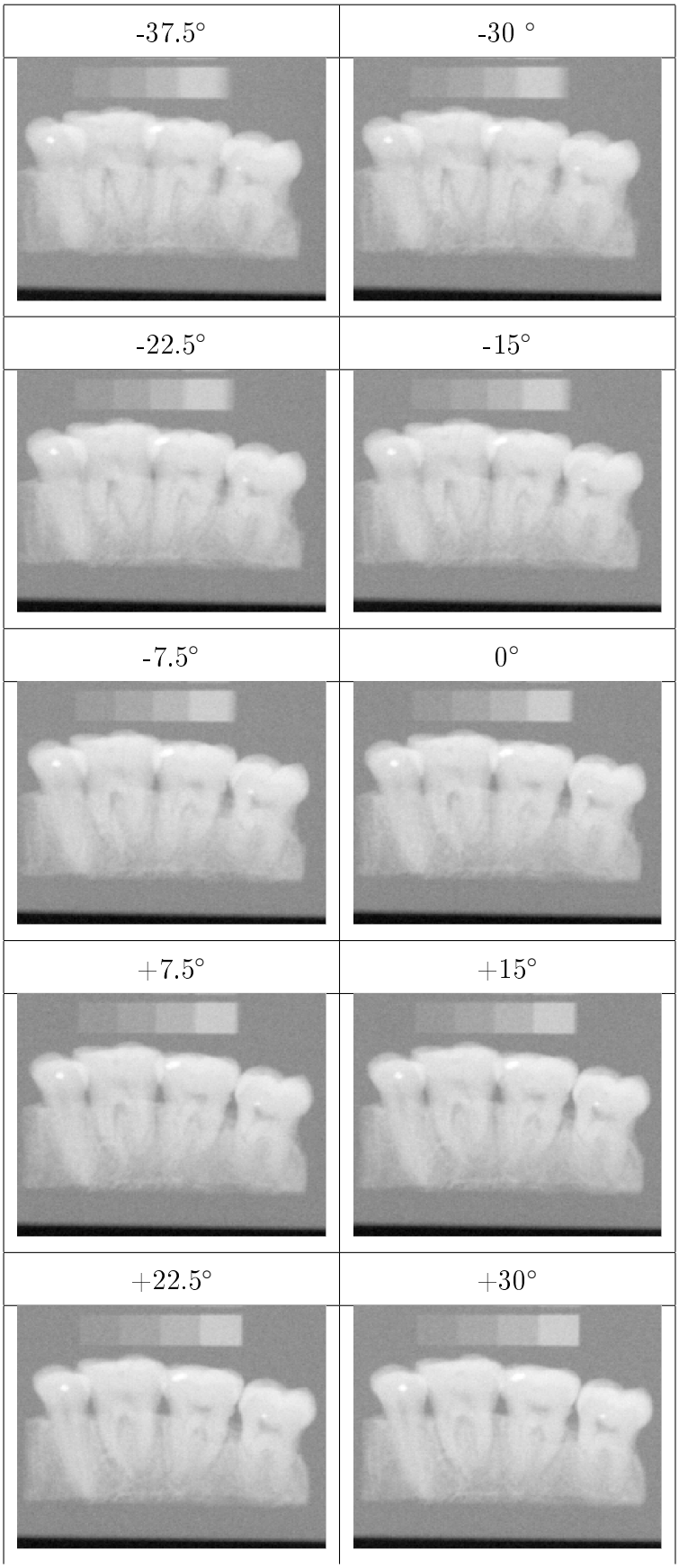

Figure 2.8 Dental Phantom Data Set

3. Results

3.1 Software Simulation Data Set

Initially The MPR algorithm that is proposed in Section 2.1 and the blur removing algorithm that is proposed in Section 2.2 are applied to the software simulation data sets that are explained in Section 2.4. Different projection groups were created for varying arc angles and acquisition steps. The resulting images are evaluated both visually and quantitatively. The quantitative evaluation method (Structural Similarity Index) is discussed in Section 2.3.

Quantitative MSSIM scores are presented in a bar graph for different projection groups.

3.1.1 Software Simulation Data Set-I

MPR algorithm and blur removal methods were applied to the data set explained in Section 2.4.1. MPR algorithm was implemented from -20mm to +20mm in the z direction for each 1mm. For every slice, the blur created by the other slices were computed and removed from the image. This process was repeated for 5 different image groups. These groups can be seen in Table 3.1.

Tomosynthesized images at slices -10mm and +10mm were selected for evaluation (Figure 3.1). Blurred and deblurred tomosynthesized images for different projection groups at these two planes are presented in Figure 3.2 and Figure 3.3.

Table 3.1
Software Simulation Data Set-I Groups

Group	Start Angle	Stop Angle	# Projections
1	-5°	+5°	2
2	-15°	+15°	4
3	-25°	+25°	6
4	-35°	+35°	8
5	-45°	+45°	10

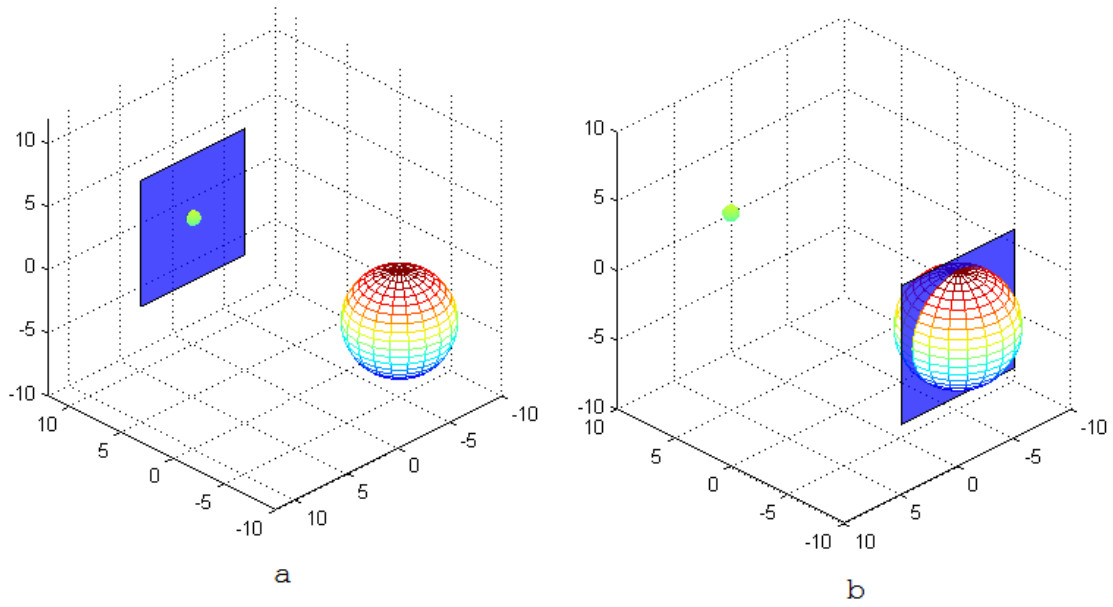

Figure 3.1 Slice positions in 3D geometry a)10mm b)-10mm

SSIM method explained in Section 2.3. was used to evaluate the correlation between the reference image and the tomosynthesized images from different projection groups. Ground truth image of the small sphere at the back from 0° was accepted as the reference image in Figure 3.4. Subsequent groups and slices in both blurred and deblurred images were also evaluated as shown in Figures 3.5 , 3.6 and Table 3.2. In both of these plots the Y-axis represents the MSSIM index acquired by comparing the reference image and the tomosynthesized plane. In case of a perfect correlation an MSSIM index of 1 is acquired. Each column

	Blurred Image	Blur Removal Applied Image
1st group (2 Projections)	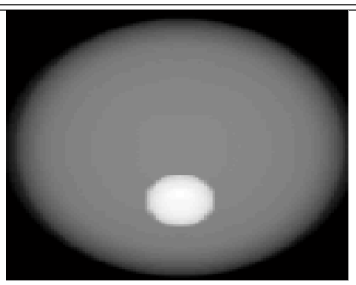	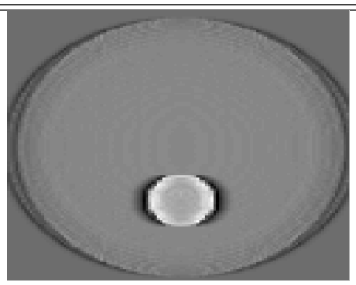
2nd group (4 Projections)	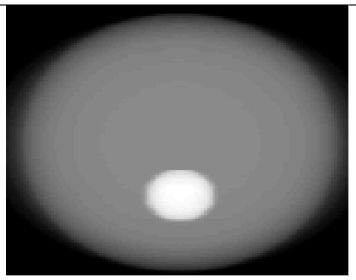	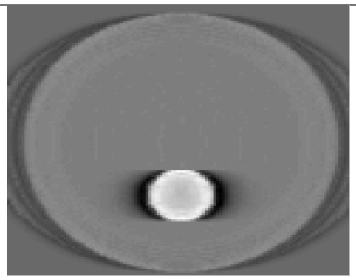
3rd group (6 Projections)	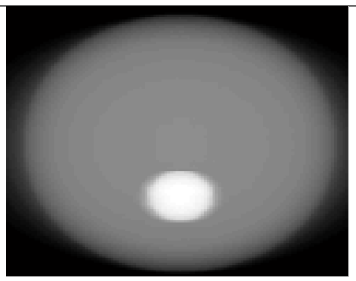	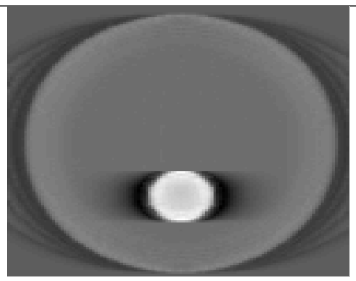
4th group (8 Projections)	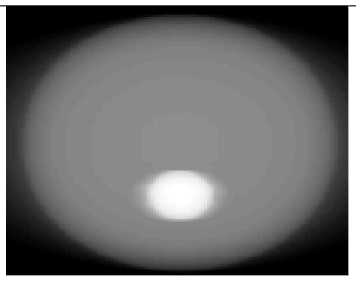	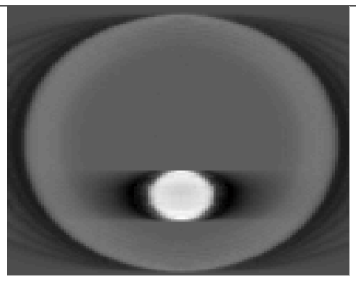
5th group (10 Projections)	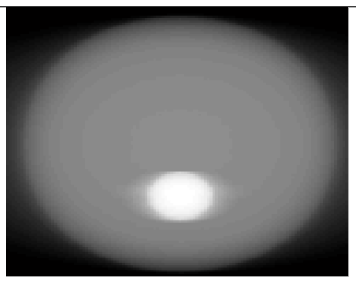	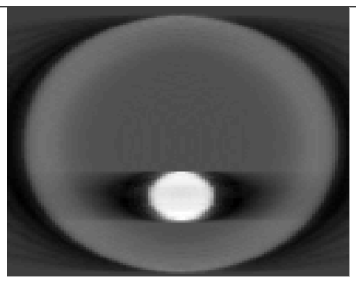

Figure 3.2 Blurred and deblurred tomosynthesized images for different projection groups at -10mm

	Blurred Image	Blur Removal Applied Image
1st group (2 Projections)	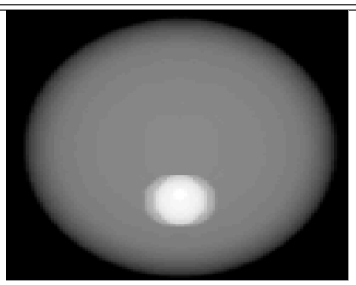	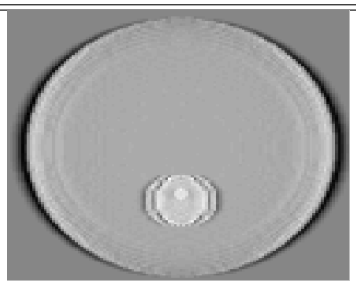
2nd group (4 Projections)	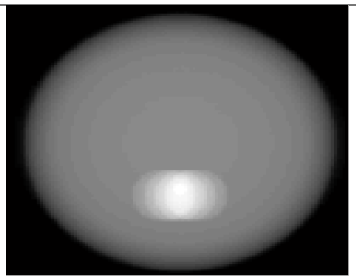	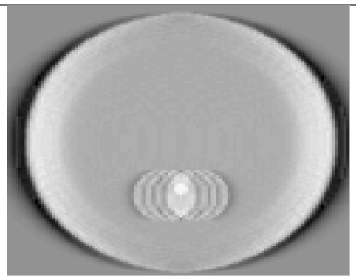
3rd group (6 Projections)	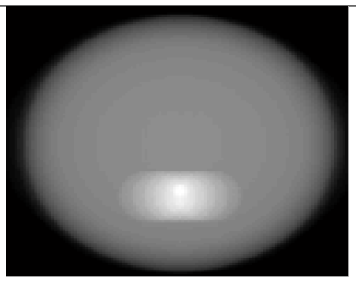	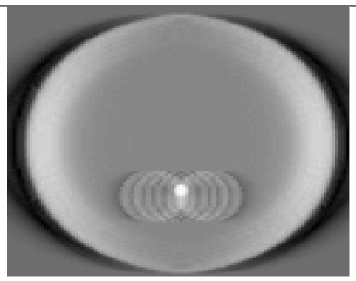
4th group (8 Projections)	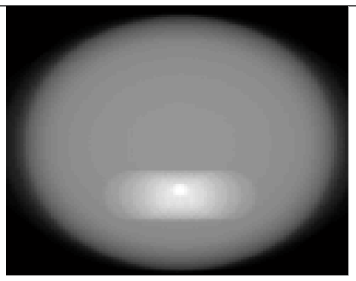	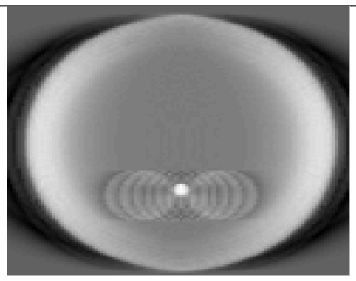
5th group (10 Projections)	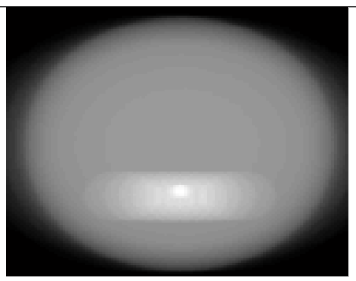	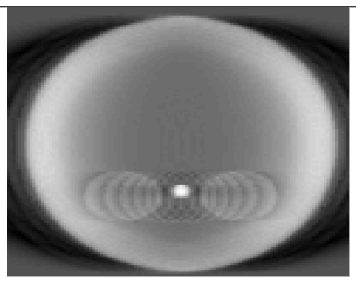

Figure 3.3 Blurred and deblurred tomosynthesized images for different projection groups at 10mm

Table 3.2
Software Simulation Data Set-I Groups

Angle°	# Projections	SSIM(Blurred)	SSIM(Deblurred)
±5°	2	0,19	0,38
±15°	4	0,22	0,50
±25°	6	0,24	0,66
±35°	8	0,32	0,71
±45°	10	0,40	0,91

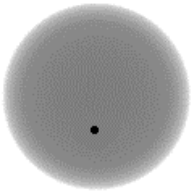

Figure 3.4 Ground truth image of the small sphere at the back from 0°

on the X-axis represents a different projection group.

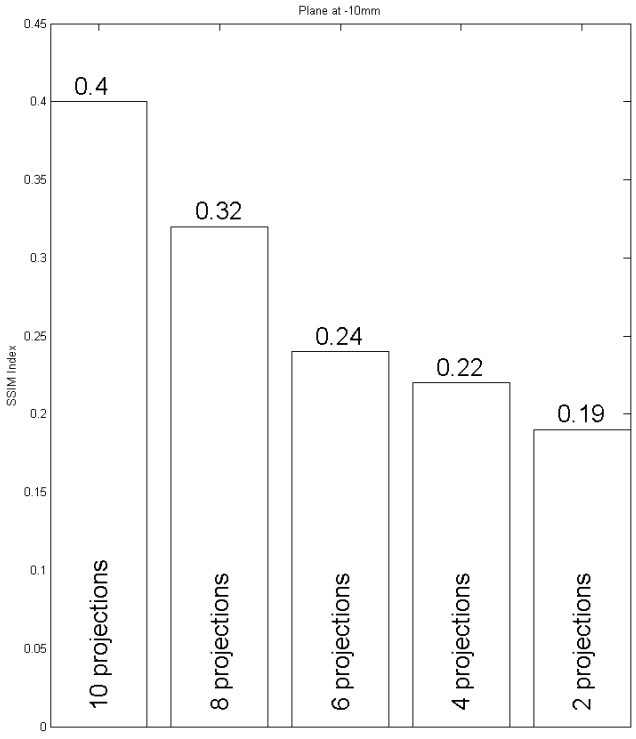

Figure 3.5 SSIM Graph for Blurred Images

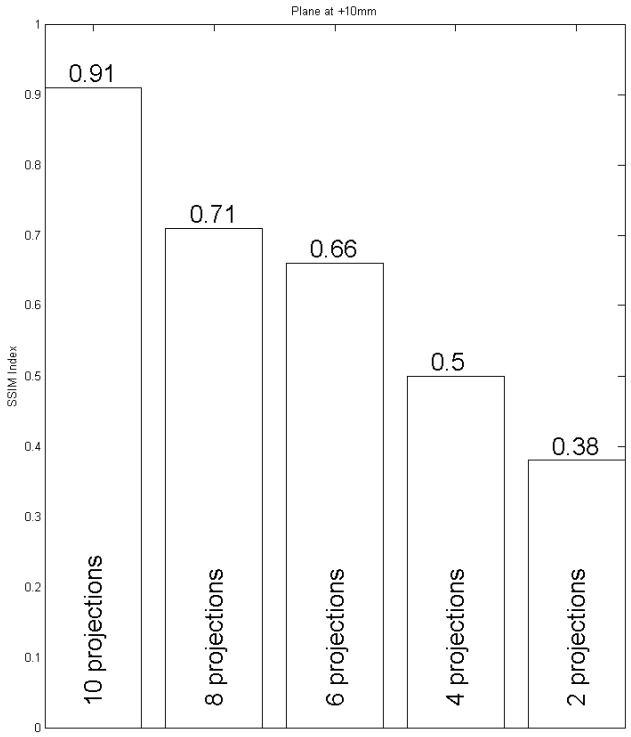

Figure 3.6 SSIM Graph for Deblurred Images

3.1.2 Software Simulation Data Set-II

MPR algorithm and blur removal methods were applied to the second data set explained in Section 2.4.2. MPR algorithm was implemented from -50mm to +60mm in the Z-axis direction for each 5mm. For every slice, the blur created by the other slices were computed and removed from the image.

This process was repeated for 12 different image groups. The method used to create different groups is described in the Table 3.3. For example for the first group; projections from -20°to +20° with 2°step difference between each projection was used. For evaluation of the image quality, the planes that correspond to the centers of the spheres are selected. These planes can be seen in Figure 3.7. The ideal projections from these planes can be seen in Figure 3.8.

All tomosynthesized images at these planes are evaluated with the ground truth image that corresponds to that particular plane. Using SSIM index the

Table 3.3
Software Simulation Data Set-II Groups

Group	Start Angle	Stop Angle	Angle Step	# Projections
1	-20°	+20°	2°	21
2	-20°	+20°	4°	11
3	-20°	+20°	8°	6
4	-16°	+16°	2°	17
5	-16°	+16°	4°	9
6	-16°	+16°	8°	5
7	-12°	+12°	2°	13
8	-12°	+12°	4°	7
9	-12°	+12°	8°	4
10	-8°	+8°	2°	9
11	-8°	+8°	4°	5
12	-8°	+8°	8°	3

results are given in Figure 3.13 and Figure 3.14 and in Table 3.4. The results show that the best MSSIM index is achieved with the largest arc and the smallest step angle.

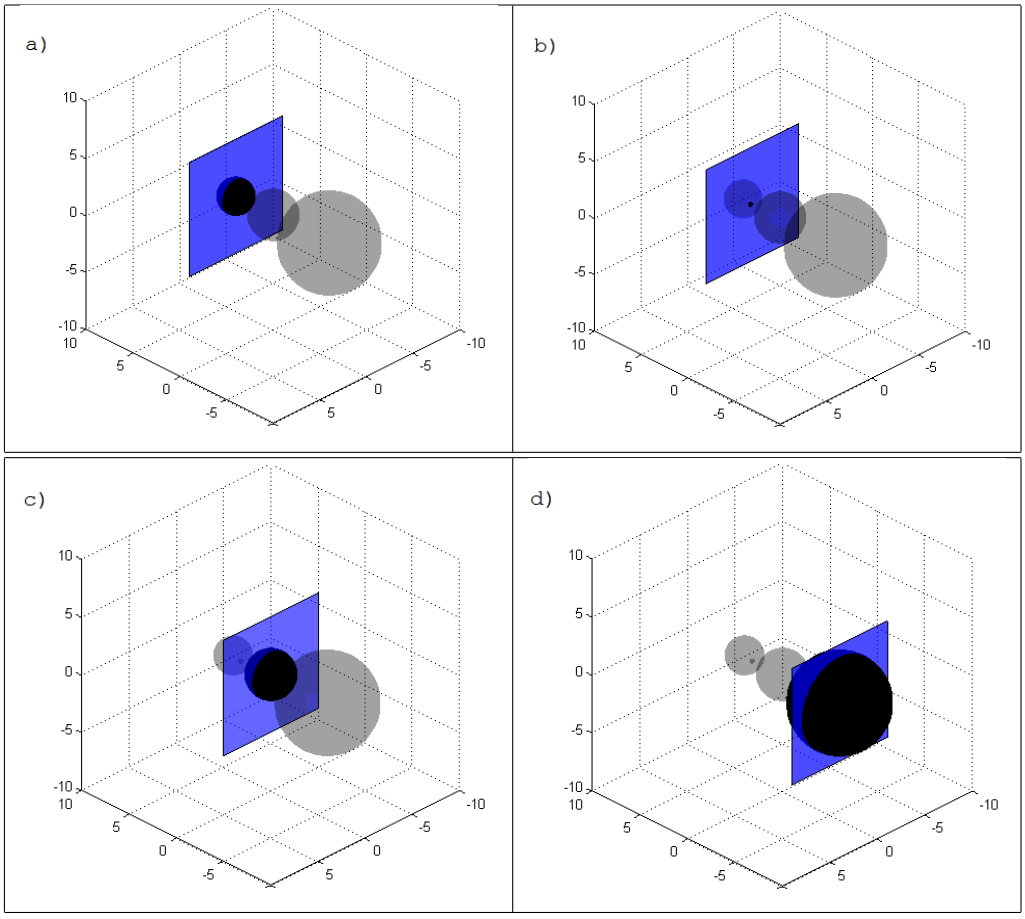

Figure 3.7 Image planes used for comparison in 3D geometry. a)-40mm b)-30mm c)0mm d)+60mm

Table 3.4
Software Simulation Data Set-II MSSIM Index a)-40mm b)-30mm c)0mm d)+60mm

Arc°	Step°	MSSIM (a)
± 20°	2°	0,64
± 20°	4°	0,5
± 20°	8°	0,45
± 16°	2°	0,58
± 16°	4°	0,45
± 16°	8°	0,44
± 12°	2°	0,52
± 12°	4°	0,41
± 12°	8°	0,40
± 8°	2°	0,46
± 8°	4°	0,40
± 8°	8°	0,43

Arc°	Step°	MSSIM (b)
± 20°	2°	0,57
± 20°	4°	0,46
± 20°	8°	0,42
± 16°	2°	0,55
± 16°	4°	0,43
± 16°	8°	0,41
± 12°	2°	0,51
± 12°	4°	0,41
± 12°	8°	0,38
± 8°	2°	0,43
± 8°	4°	0,38
± 8°	8°	0,41

Arc°	Step°	MSSIM (c)
± 20°	2°	0,64
± 20°	4°	0,48
± 20°	8°	0,41
± 16°	2°	0,62
± 16°	4°	0,43
± 16°	8°	0,36
± 12°	2°	0,59
± 12°	4°	0,42
± 12°	8°	0,35
± 8°	2°	0,54
± 8°	4°	0,42
± 8°	8°	0,39

Arc°	Step°	MSSIM (d)
± 20°	2°	0,58
± 20°	4°	0,55
± 20°	8°	0,51
± 16°	2°	0,59
± 16°	4°	0,55
± 16°	8°	0,50
± 12°	2°	0,64
± 12°	4°	0,57
± 12°	8°	0,50
± 8°	2°	0,65
± 8°	4°	0,58
± 8°	8°	0,54

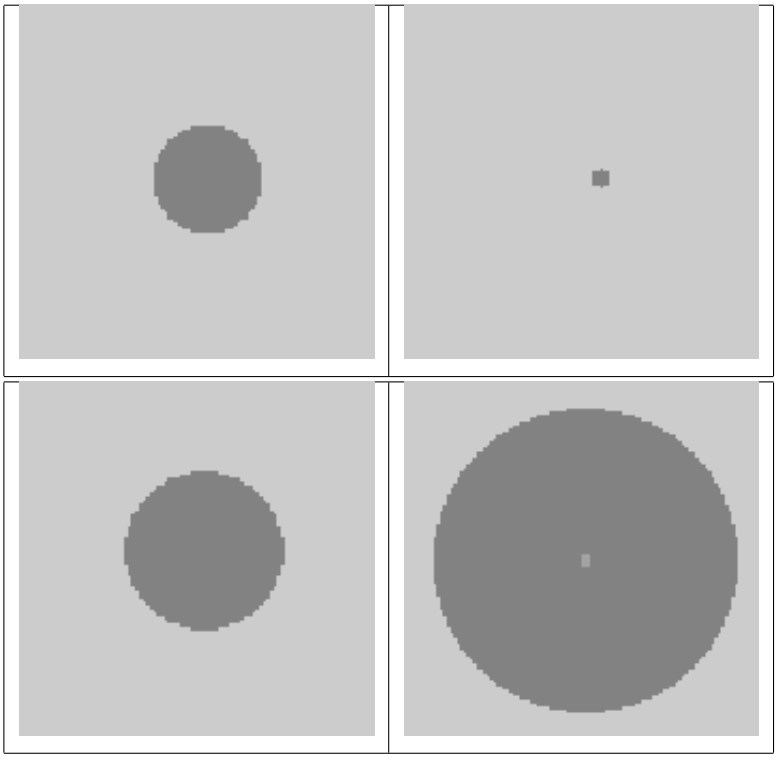

Figure 3.8 Image plane projections used for comparison. a)-40mm b)-30mm c)0mm d)+60mm

3.2 Dental Phantom Data Set

The phantom used to obtain this data set is a Gammex 501A dental phantom. It consists of three real molar teeth and one pre-molar tooth inside the jawbone. A Siemens CT system was used to obtain these projections. The source-detector distance is 1200mm and source-isocenter distance is 750mm. The images are acquired with an arch of $\pm 200^{\circ}$ with 1.5°intervals. The raw data containing all projections from these angles are used in the MPR algorithm. The acquisition arc angle is limited to $\pm 20^{\circ}$ since it is a physically realistic acquisition arc in clinical dental imaging. Back-projected data is used to create tomographical slice planes. Four of these planes that show characteristic dental structures are selected for comparison with the corresponding tomosynthesized planes. These planes can be seen in Figure 3.15.

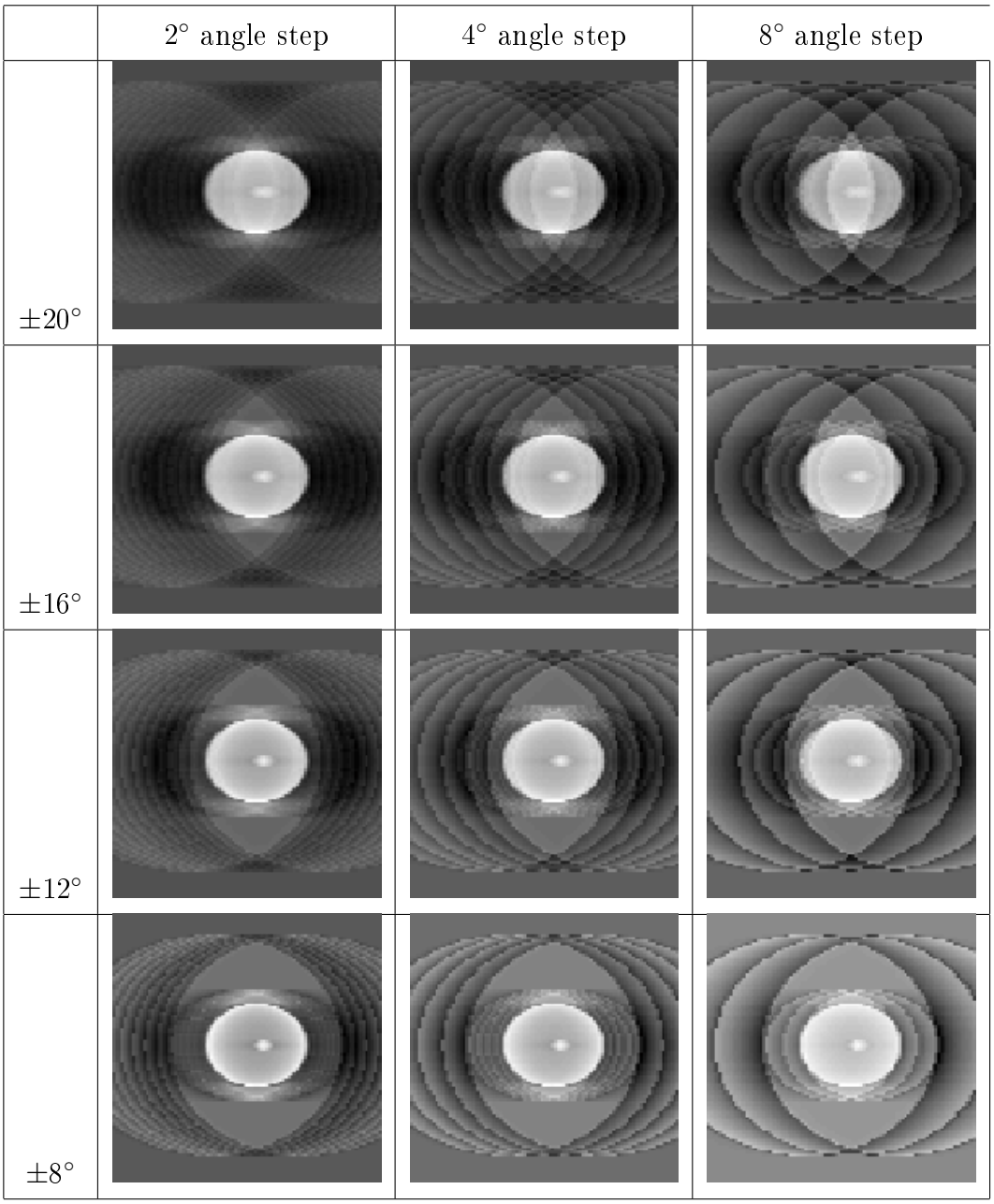

Figure 3.9 Tomosynthesized images at plane -40mm for varying arc (rows) and step angles (columns)

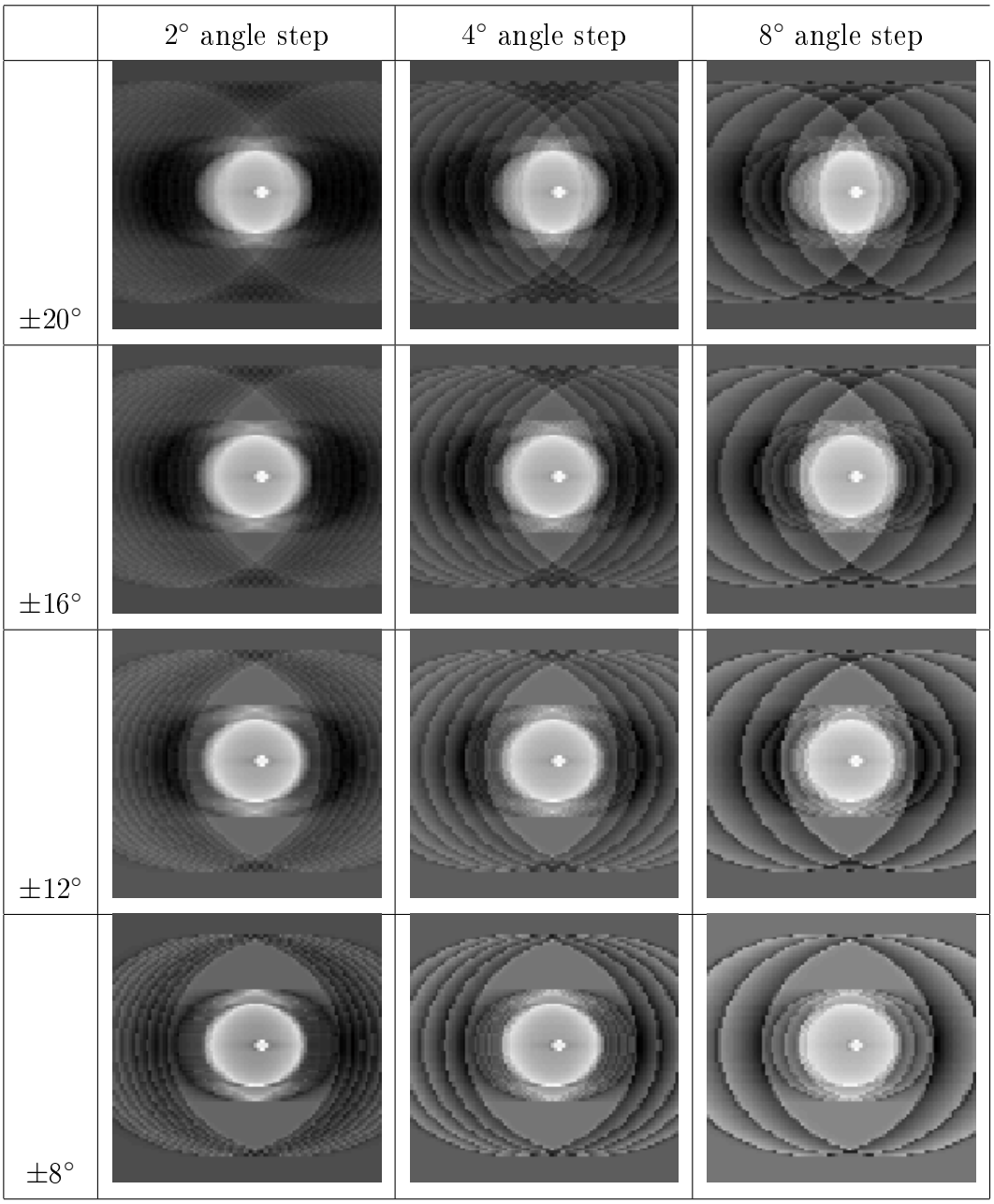

Figure 3.10 Tomosynthesized images at plane -30mm for varying arc (rows) and step angles (columns)

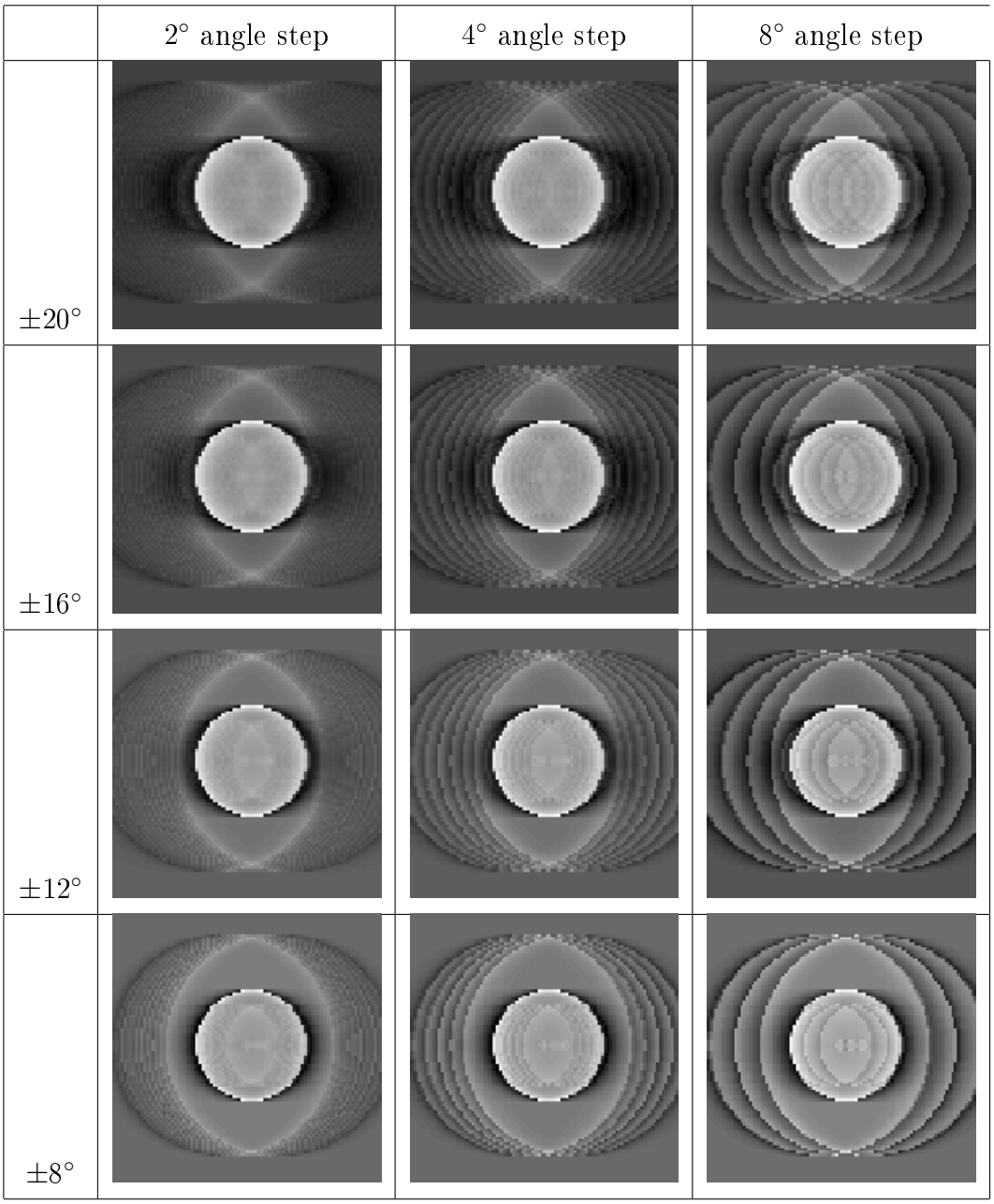

Figure 3.11 Tomosynthesized images at plane 0mm for varying arc (rows) and step angles (columns)

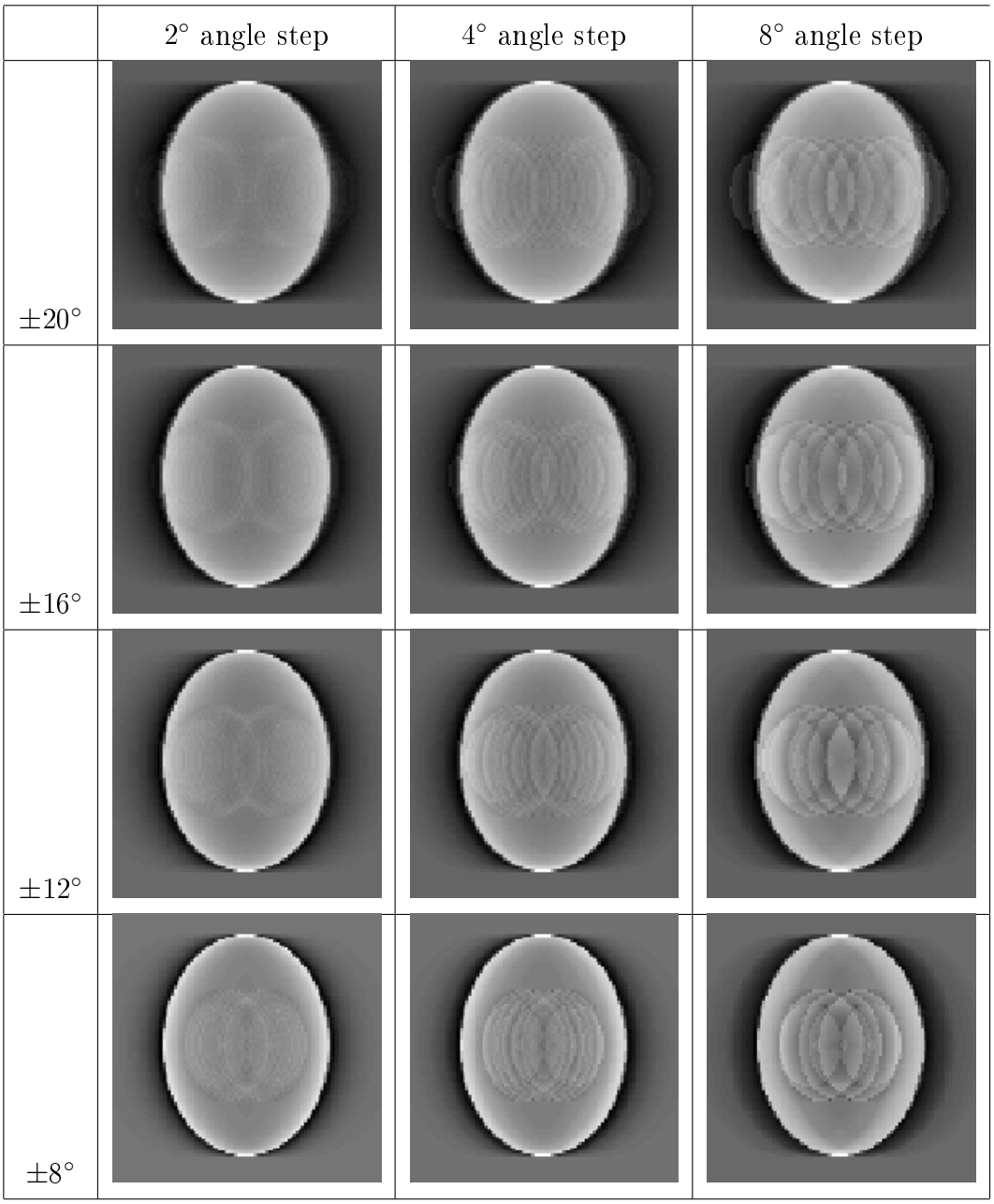

Figure 3.12 Tomosynthesized images at plane +60mm for varying arc (rows) and step angles (columns)

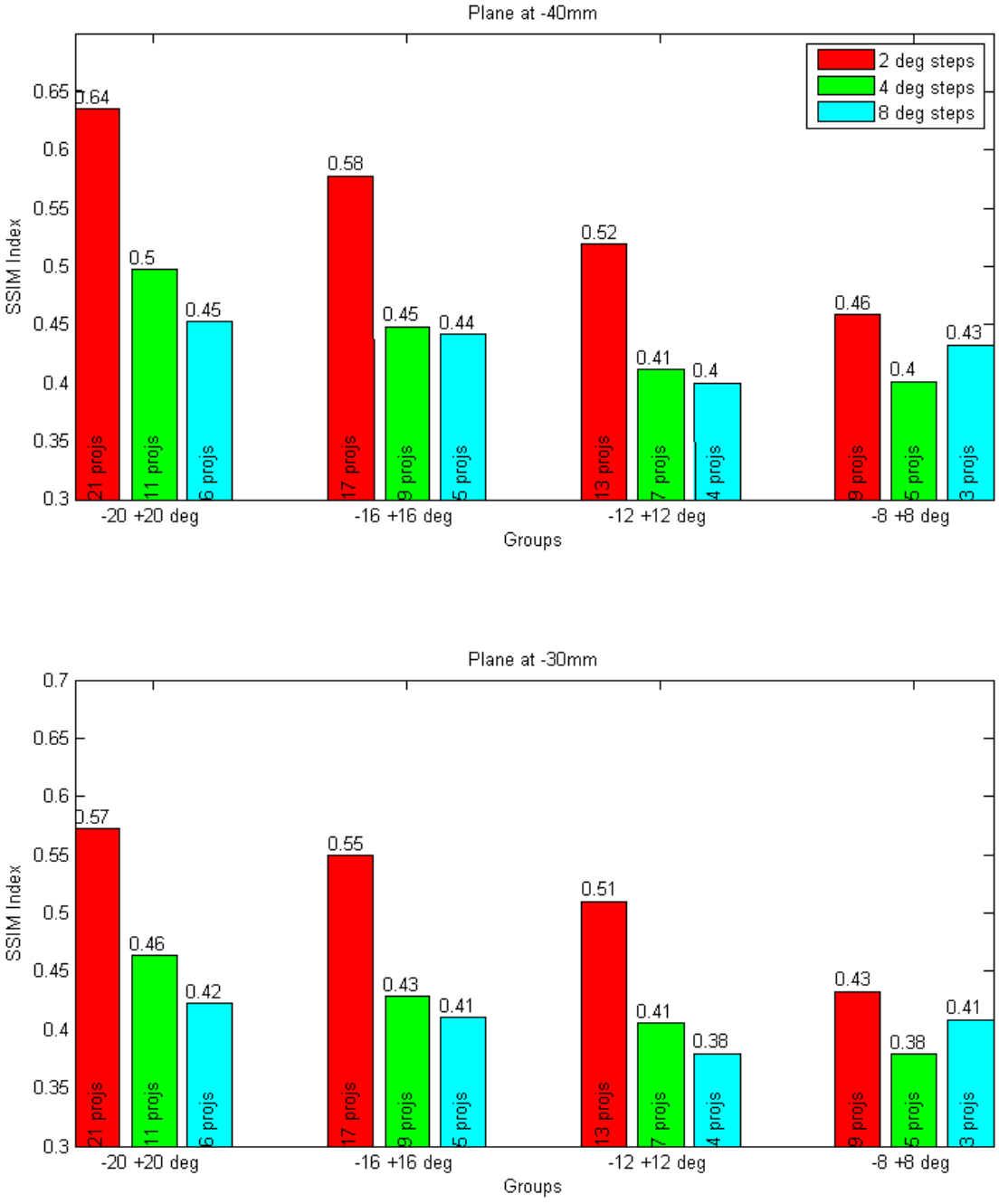

Figure 3.13 SSIM Graph for Deblurred Images

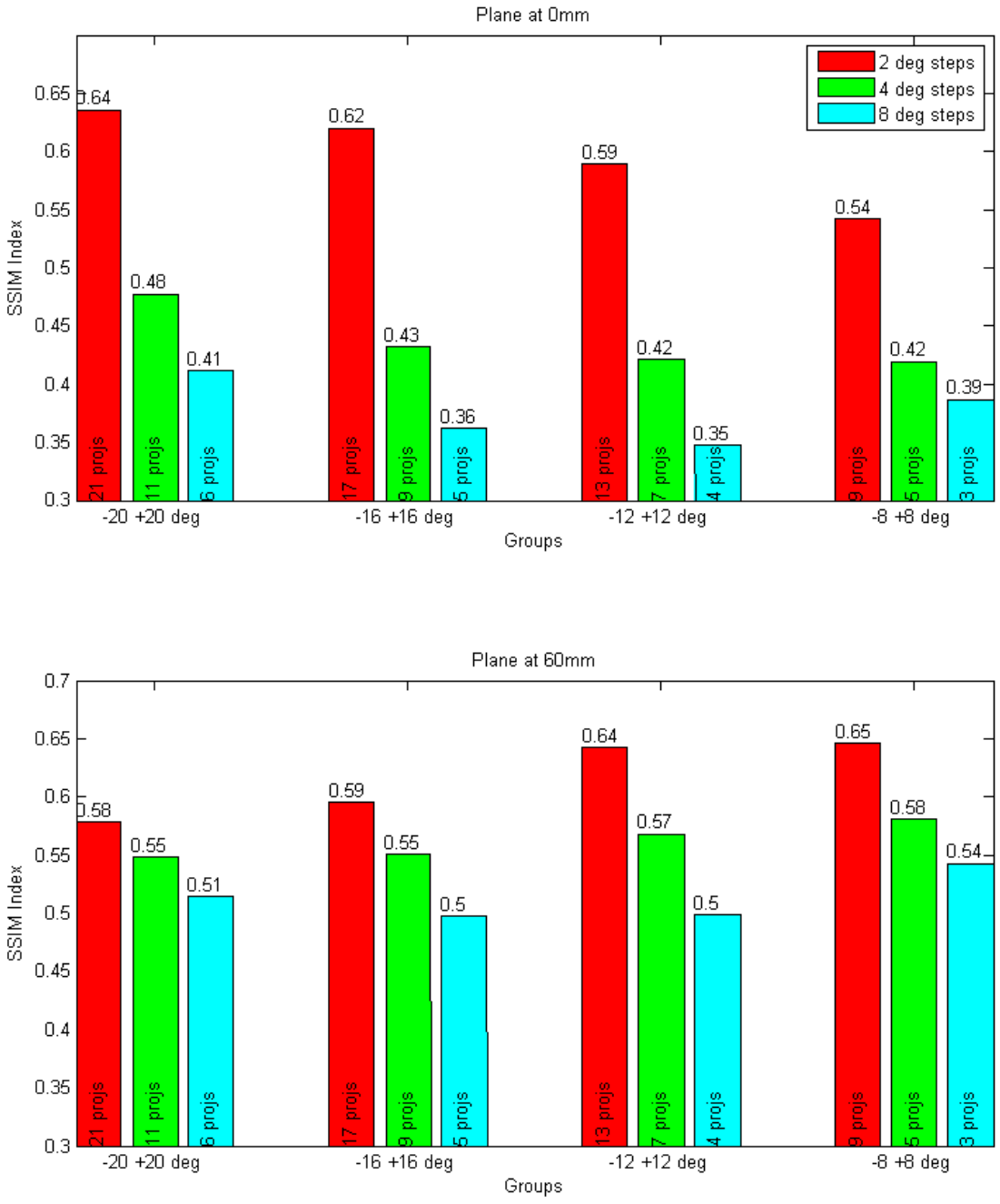

Figure 3.14 SSIM Graph for Deblurred Images

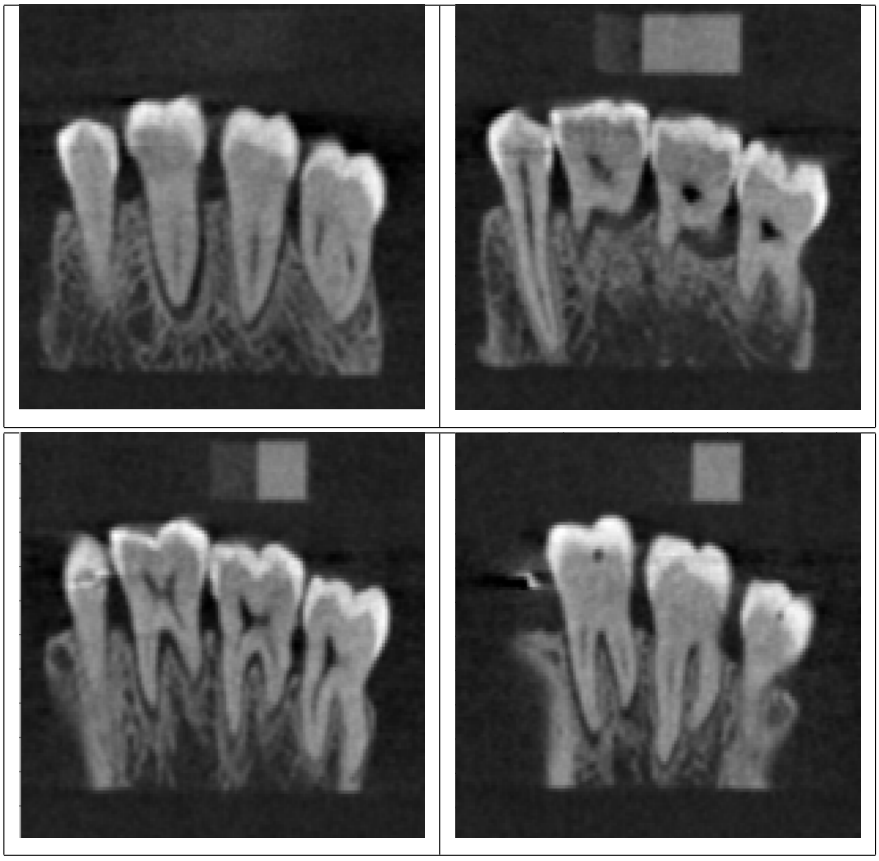

Figure 3.15 Image plane projections used for comparison. a)4mm b)8mm c)11mm d)13mm

The 3D model created from the back-projection data is used for further visual evaluation (Figure 3.16)

12 different image groups were created. The method used to create different groups is described in the Table 3.5. For example for the first group; projections from -22°to +23° with 1.5° step difference between each projection was used, therefore total of 30 images were used to create tomosynthesis image. For evaluation of the image quality, four particular tomographical planes were selected that have some characteristic features (roots, canals, dents) and these tomographic planes were compared to the particular tomosynthesized planes in each group. Tomosynthesized planes can be seen in Figures 3.19,3.20,3.21,3.22.

MPR algorithm and blur removal methods were applied to the data set

Figure 3.16 3D model of the dental phantom.

explained in Section 2.5. MPR algorithm was implemented from -5mm to +17mm in the z direction for each 0.3mm. For every slice, the blur created by the other slices were computed and removed from the image. Image planes from 4mm to 13mm with 1mm step size in the Z-direction for both blurred and deblurred results for the 1st group are shown in Figure 3.17 and Figure 3.18.

Side by side comparison of the tomographical and tomosynthesized planes shows that anatomical structures at different depths can be distinguished. In Figure 3.23 the canals in the molar teeth and the single roots of these teeth are visible. In Figure 3.24 the canal in the pre-molar teeth and its root is focused. In the molar teeth the focus plane crosses the pulp of the teeth. In Figure 3.25 the focus plane is deeper and it allows us to see the canals in the molar teeth and the double roots of these teeth. In Figure 3.26 the focus plane is at its deepest. At this depth the cavities in the teeth can be distinguished.

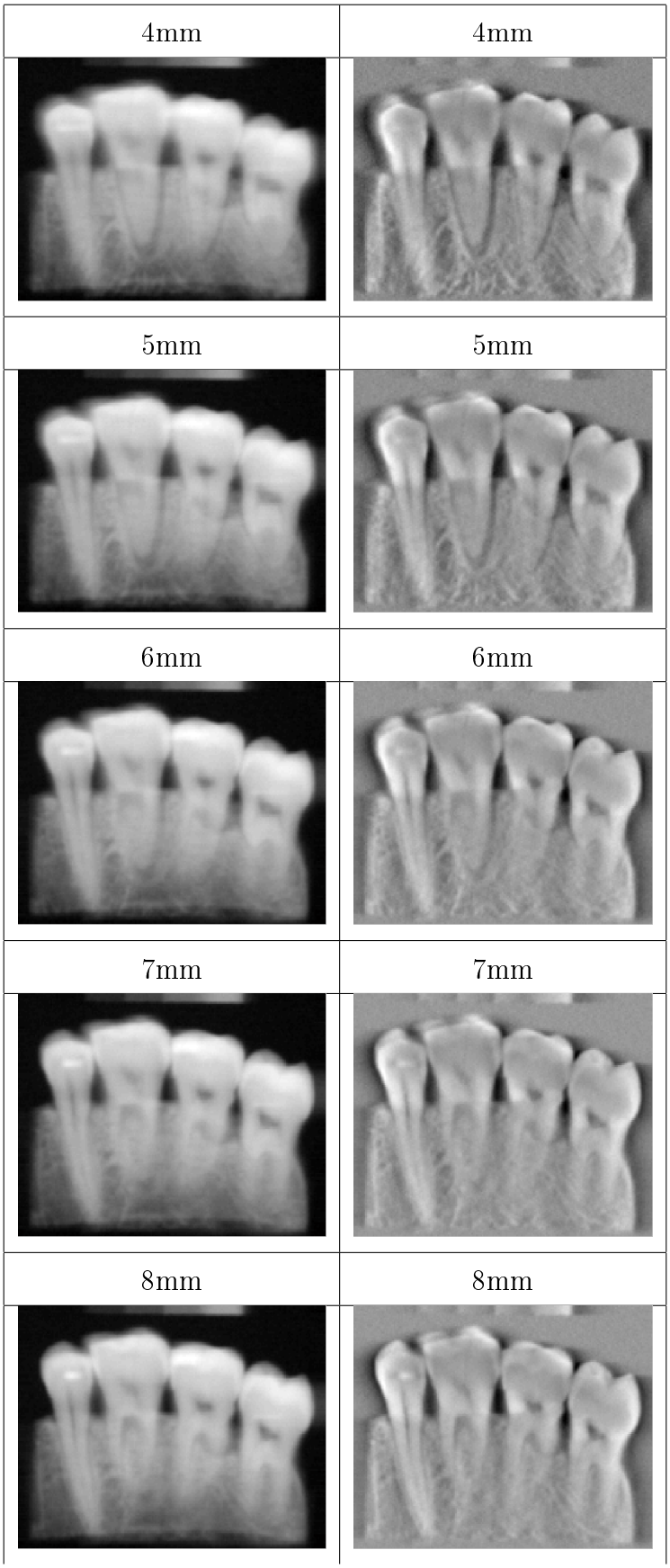

Figure 3.17 Tomosynthesized planes between 4mm-8mm in Dental Phantom Data Set (Right=Blurred, Left=Deblurred).

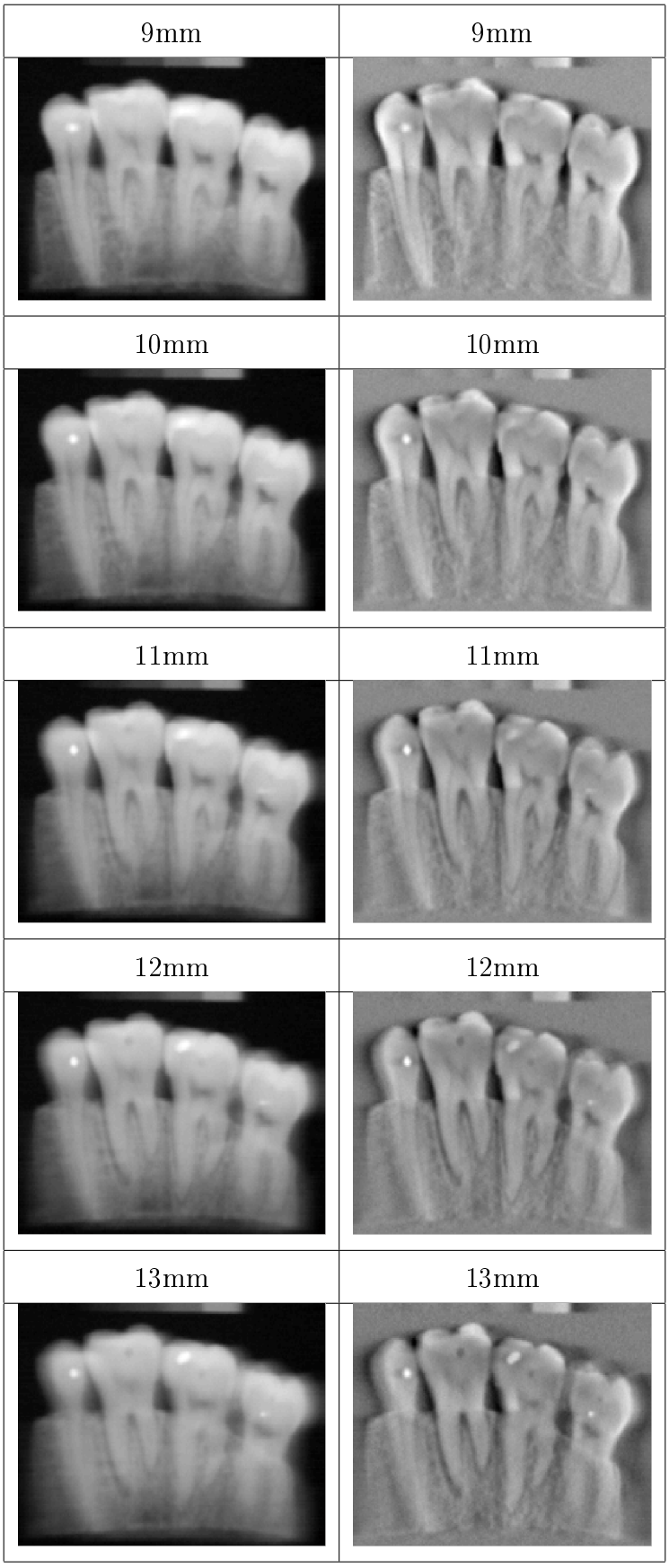

Figure 3.18 Tomosynthesized planes between 9mm-13mm Dental Phantom Data Set (Right=Blurred, Left=Deblurred).

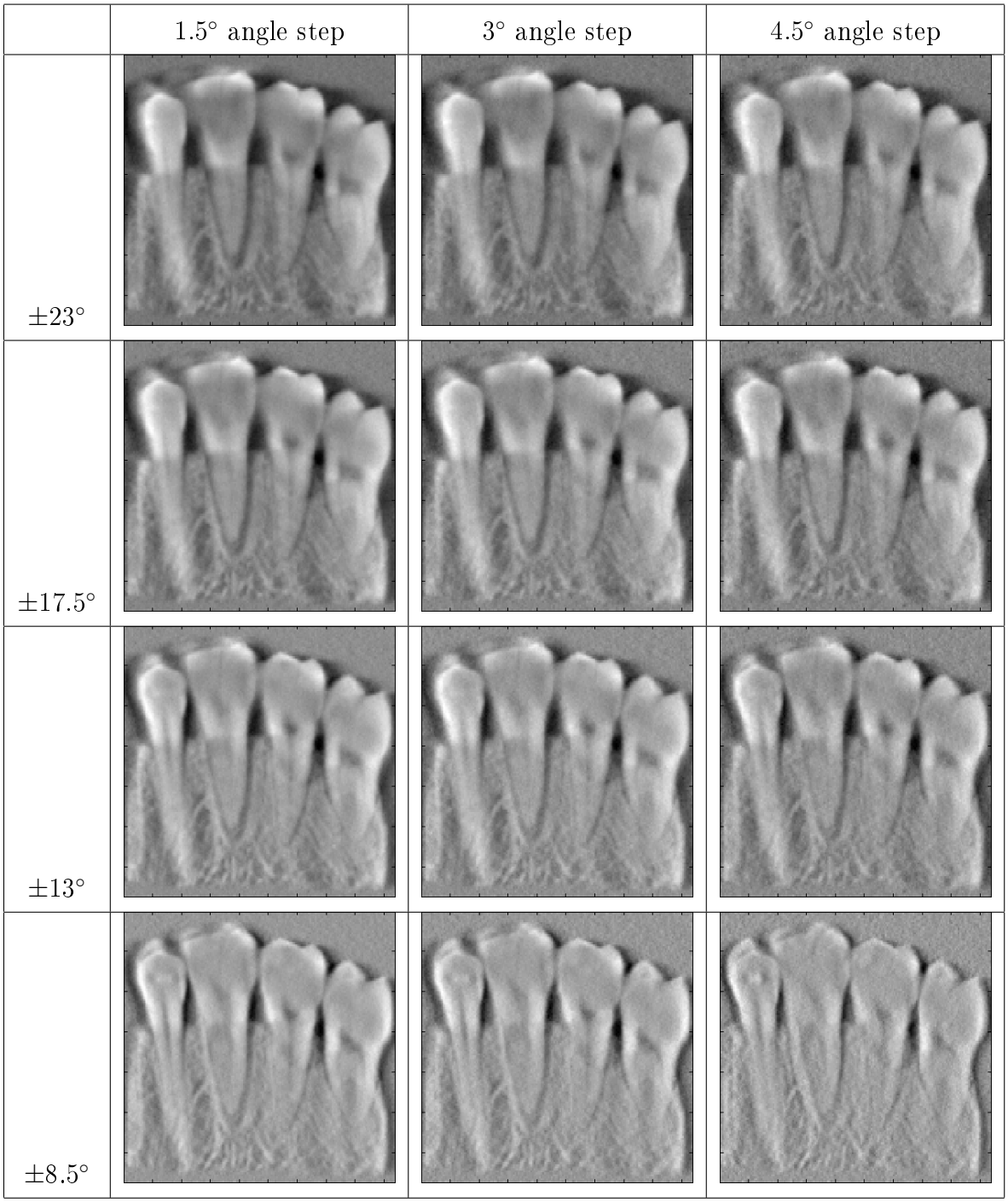

Figure 3.19 Tomosynthesized images at 4mm for varying arc (rows) and step angles (columns).

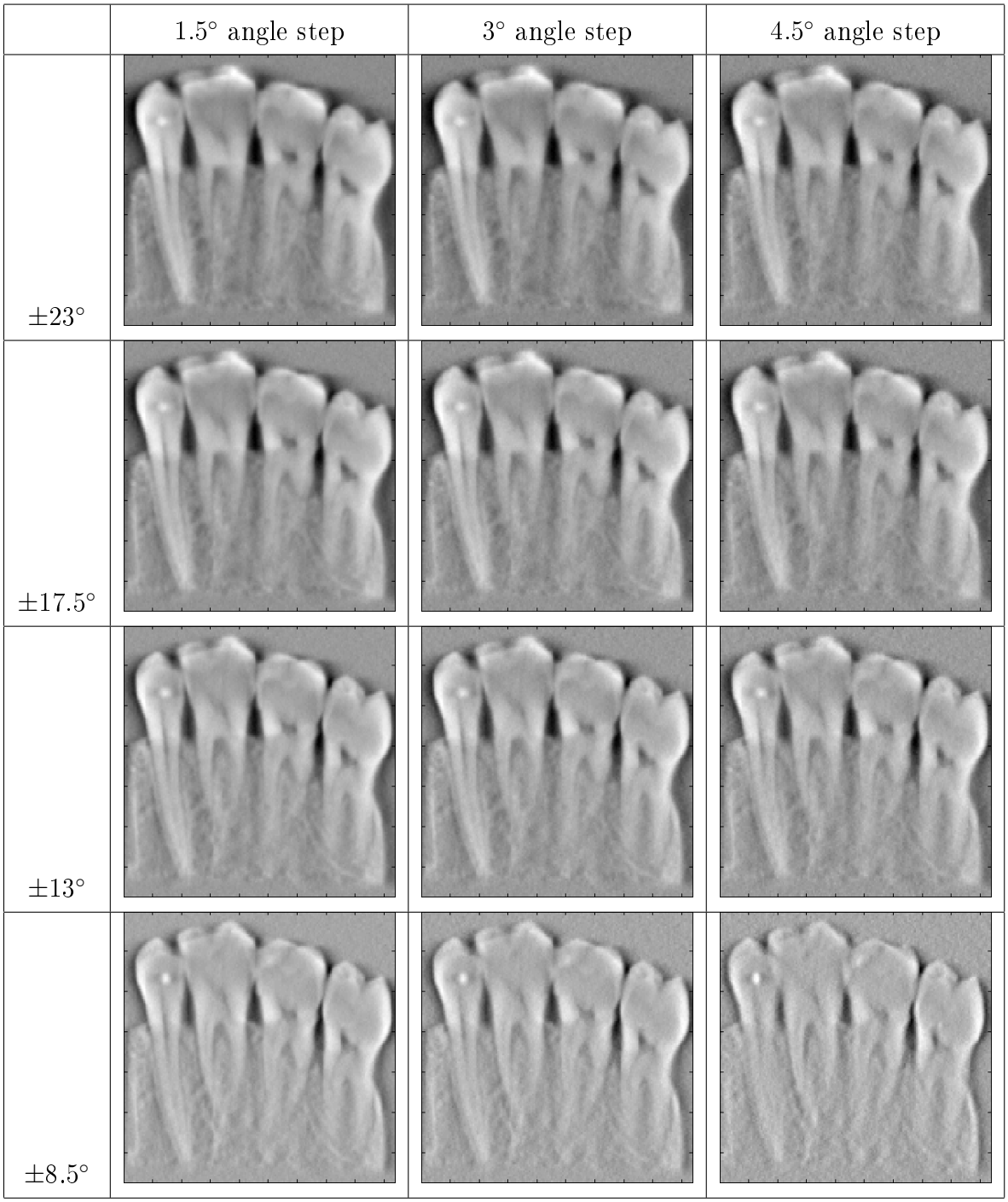

Figure 3.20 Tomosynthesized images at 8mm for varying arc (rows) and step angles (columns).

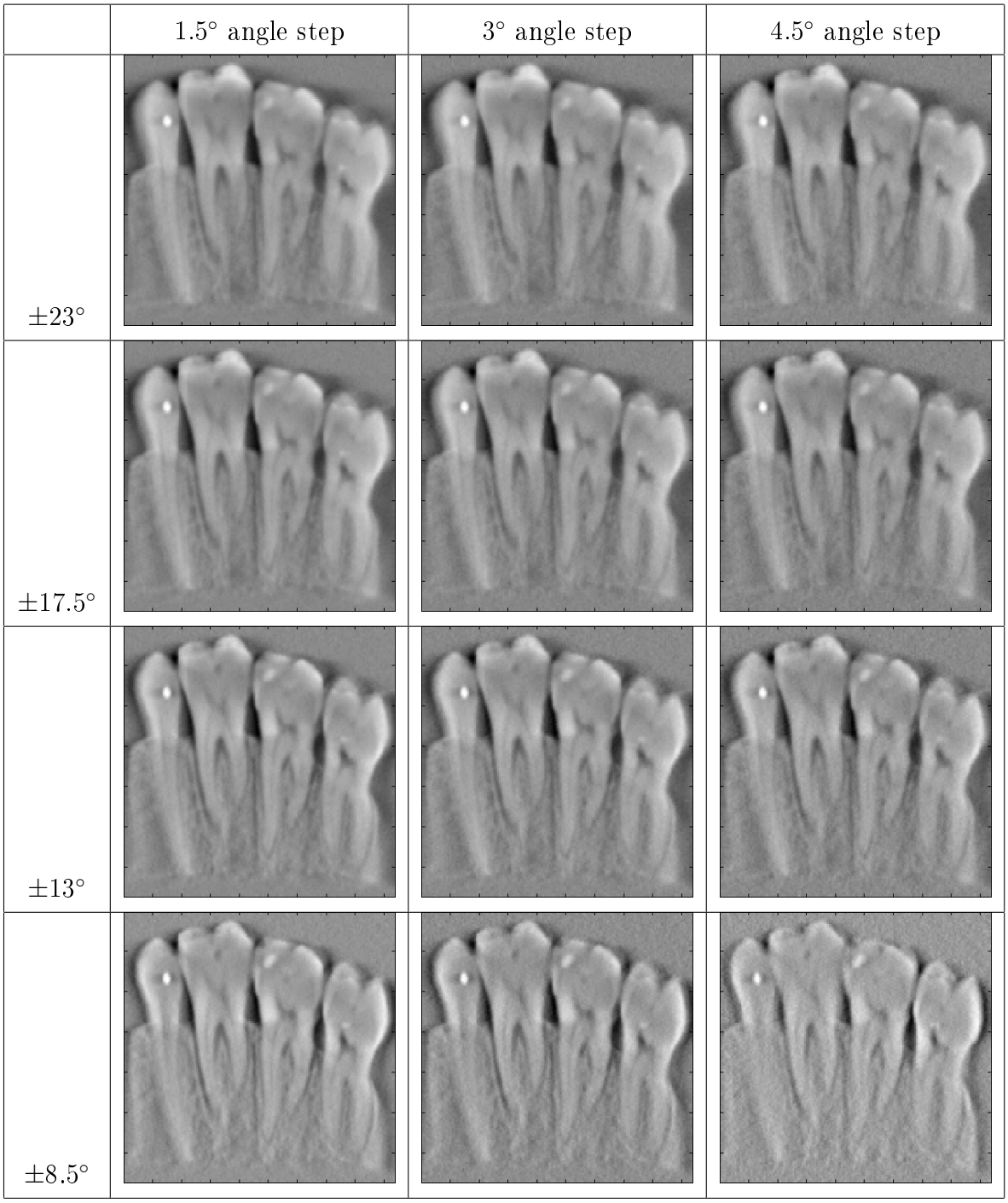

Figure 3.21 Tomosynthesized images at 11mm for varying arc (rows) and step angles (columns).

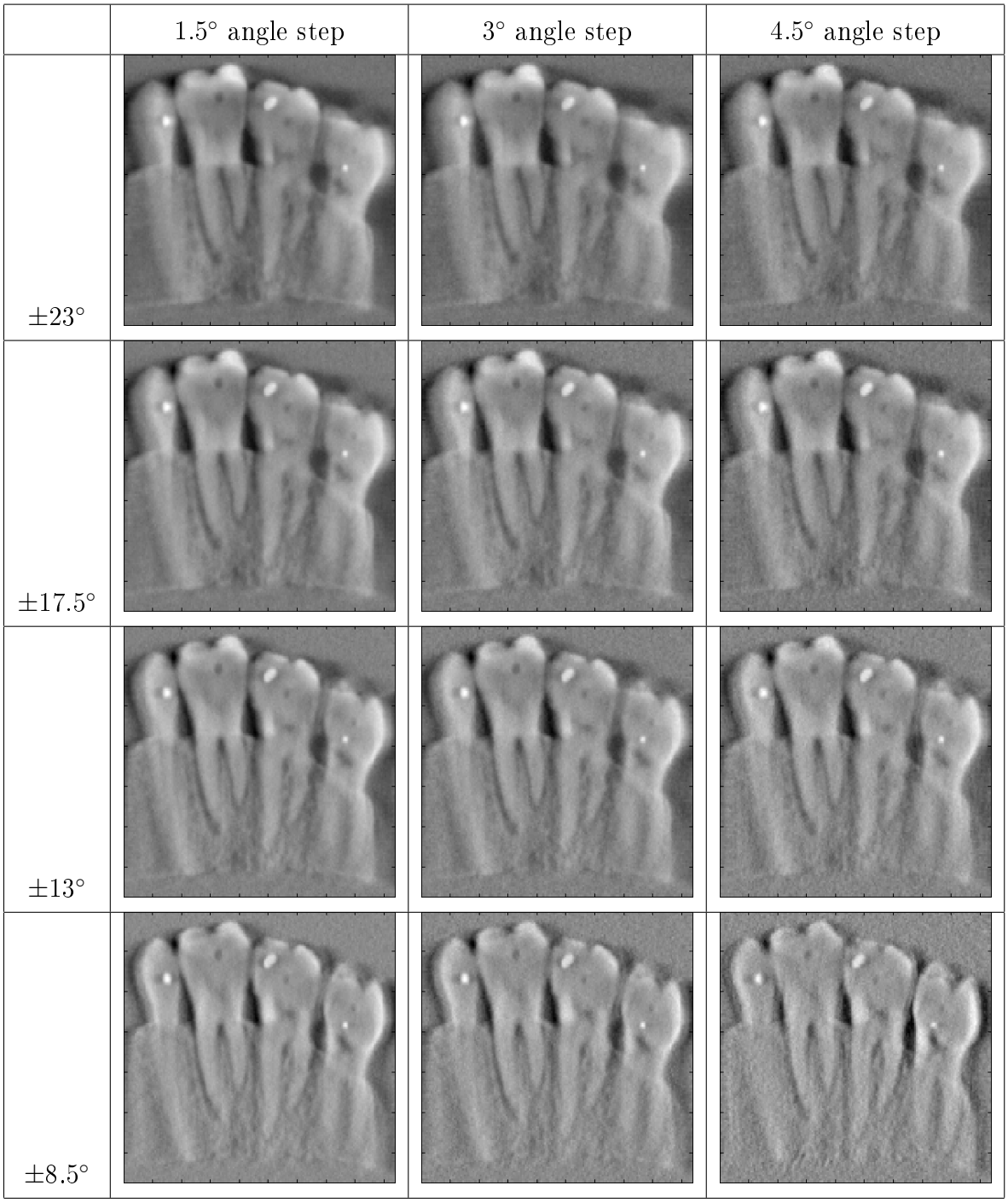

Figure 3.22 Tomosynthesized images at 13mm for varying arc (rows) and step angles (columns).

Table 3.5
Dental Phantom Data Set Projection Groups

Group	Start Angle	Stop Angle	Angle Step	# Projections
1	-22°	+23°	1.5°	30
2	-22°	+23°	3°	16
3	-19°	+20°	4.5°	10
4	-17.5°	+18.5°	1.5°	24
5	-17.5°	+17°	3°	12
6	-17.5°	+15.5°	4.5°	8
7	-13°	+14°	1.5°	18
8	-13°	+14°	3°	10
9	-13°	+11°	4.5°	6
10	-8.5°	+9.5°	1.5°	12
11	-8.5°	+8°	3°	6
12	-10°	+11°	4.5°	4

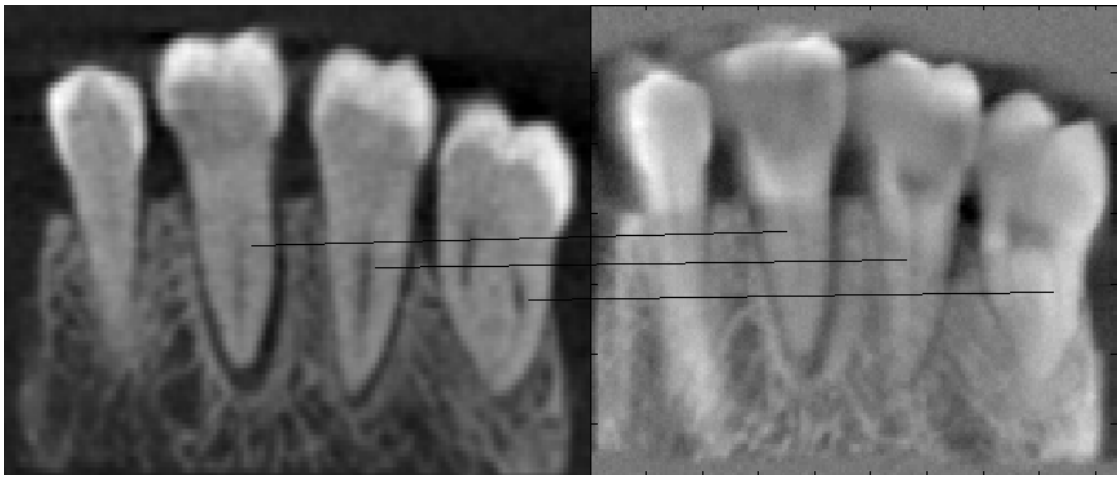

Figure 3.23 Comparison of tomographical and tomosynthesized planes at 4mm.

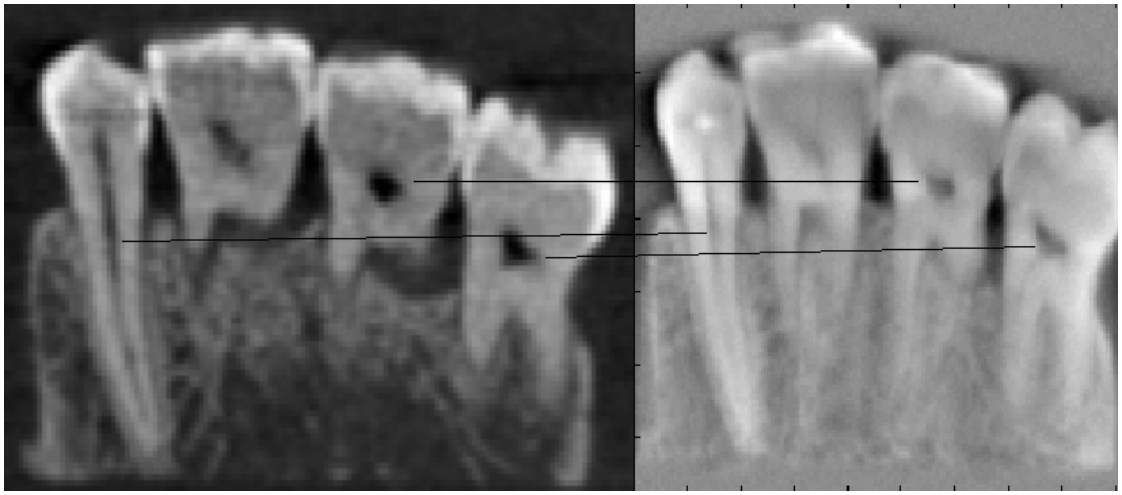

Figure 3.24 Comparison of tomographical and tomosynthesized planes at 8mm.

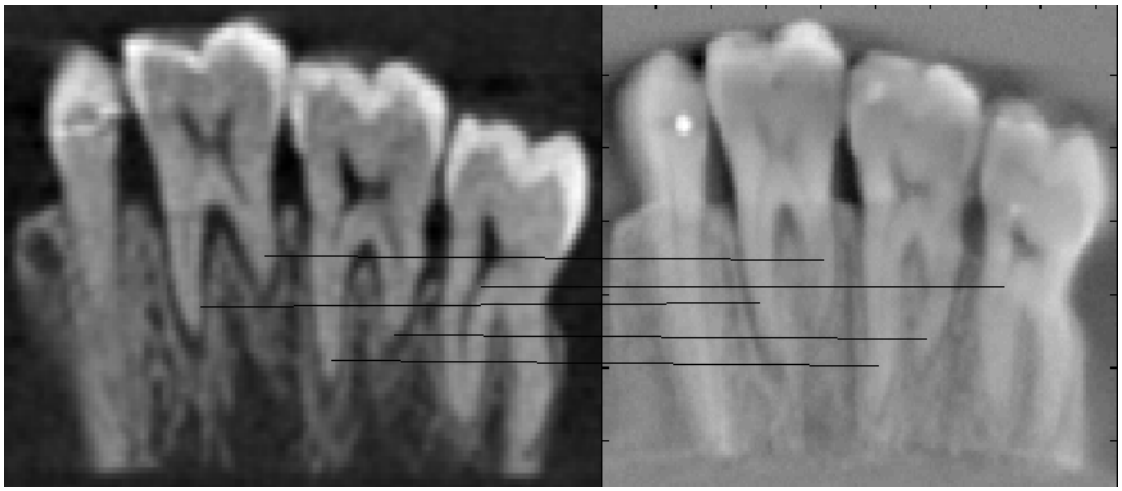

Figure 3.25 Comparison of tomographical and tomosynthesized planes at 11mm.

Figure 3.26 Comparison of tomographical and tomosynthesized planes at 13mm.

4. Discussion

In the thesis, a multiple projection reconstruction algorithm was used to reconstruct limited angle tomographic images. Simulation data set results presented in Section 3.1.1 showed that, increasing projection arc and image count helped increasing the contrast and the visibility of the object on the target plane. Additionally application of the blur removal method further increased the level of the image quality. Image quality was evaluated using the ground truth images of the simulation, for the data set I. This was the cross-sectioned image of the small sphere at the back from 0°angle. Blurred tomosynthesis images showed an increasing SSIM index as the projection arc and image count increased. A maximum SSIM index of 0.4011 was achieved with the blurred data set using all the 10 images around the arc of ±45°for the simulation data set I.

SSIM evaluation of the ground truth image of the small sphere at the back from 0°angle with the deblurred images showed the similar characteristic as the blurred images. That is increasing SSIM index as the projection arc and image count increased. A maximum SSIM index of 0.9184 was achieved with the deblurred data set using all the 10 images around the arc of ±45° (Table3.2).

SSIM evaluation of the simulation data set showed that the best results in both blurred and deblurred images were achieved by increasing the projection arc and image count. Additionally, SSIM index of the deblurred images were more than the double of the SSIM index of the blurred images.

SSIM index was also used with the second simulation data set described in Section 2.4.2. The projection angle and the step angle difference are varied among groups. Initially four different groups are created with the projection arc angle of (-20°+20°), (-16°+16°), (-12° +12°), (-8°+8°). The projections acquired with three different angle step sizes of 2°, 4° and 8°were used in each of these

groups. SSIM index was evaluated for each of these 12 groups using the ground truth cross sectioned image of that particular plane through the virtual phantom.

Results in Table 3.4show that using 2° angle step size had the greatest SSIM index among the groups. Also as expected, SSIM index was increased with the increase of acquisition arc angle. So the greatest SSIM index is achieved by using an acquisition arc of -20°to +20°.

The MPR algorithm was also used to reconstruct the physical dental phantom images. These images were taken in a clinical CT scanner around an arc of ±100°. The projection angle and the step angle difference are varied among groups. Initially four different groups are created with the projection arc angle of (-22°+23°), (-17.5°+17°), (-13° +11°), (-8.5°+9°). Three sub-groups were created in this groups with projections taken with three different angle step sizes of 1.5°, 3° and 4.5°were used in each of these groups (Table 3.5). Blur removal method was also applied to blurred images. Four particular planes are selected along the Z-axis in each of the 12 groups. Visual comparison of the tomosynthesized planes in these groups are compared to the corresponding tomographically reconstructed planes. Visual evaluation of the tomosynthesized planes in Figures 3.19, 3.20, 3.21, 3.22 showed that different anatomical structures or anomalies (roots, canals, dents) at different plane of interests can be identified similar to those particular tomographical planes.

As the angle of the acquisition arc increases, out-of-plane resolution increases; however the in-plane resolution decreases. In short with wider angle acquisitions, the out-of-plane structures interference decrease but the object in the plane loses its sharpness. A larger scan angle can broaden the object, decreasing the resolution and sharpness of objects in the slice.

Similarly increasing the projection count by decreasing the step angle between the projections along a fixed acquisition arc; results in images with less

tomographic noise (artifacts). All additional projection increases the object contrast at the focus plane and reduces the out-of-plane blurring. However acquiring more projection inevitably means more radiation and calculation time. That's why increasing the projection count after a certain number is not preferable as it would not add further value to the image quality and expose the patient to unnecessary radiation.

5. Conclusions

The results of this work have shown that tomosynthesis can be successfully applied to dental X-ray imaging using an isocentric configuration. Digital tomosynthesis allows the focusing on single selected planes throughout the volume of the software simulation or dental phantom. It can remove structures outside the target plane and sharpen the contrast of the wanted structure, preventing the obscuration of the target plane as it happens in a single projection imaging. Digital tomosynthesis also enhances the contrast of less dense features, while removing denser features located in planes outside the target plane.

Digital tomosynthesis allows the physician to evaluate the dental structures almost in a volumetric fashion. The patient on the other hand is not exposed to excess radiation to acquire this 3D information since the digital tomosynthesis method uses projections in only a limited angle range in comparison to CT where a full angle acquisition is required.

6. Future Works

In this thesis we implemented an MPR algorithm and a blur removal method. We tested this algorithm with two simulation phantom data sets and a dental phantom. We studied the effects of deblurring process, changes in parameters (acquisition arc, step angle). We presented qualitative and quantitative results for these different parameters. Although a feasibility of this method is shown for dental X-ray imaging, a lot of additional work needs to be completed before any clinical implementation.

These future additional work could be summarized in these following bullets:

1. Quantify, in details with finer increments, the dependence on number of planes, angle span, number of projections, radiation exposure per projection.
2. Investigate the use of different X-ray spectra by differentiating the variables, KVp, mA and second.
3. Compare the efficiency in terms of radiation dose and image quality of digital tomosynthesis with other dental imaging techniques namely, Intra-oral, panoramic and cone-beam CT of the head.
4. Develop a mechanical system to capture the digital dental X-ray images along a circular arc using a stationary intra-oral dental sensor.
5. Develop the algorithm so that it can be implemented to be used with the proposed mechanical system.
6. Develop a graphical user interface that controls the source and the sensor to capture, to process and to display the images in a clinical environment with ease.

Bibliography

1. B. Bowers. *X-rays: their discovery and applications.* Science Museum booklet. H.M.S.O., 1970.

2. G.F. Barker, W.C. Röntgen, G.G. Stokes, and J.J. Thomson. *Röntgen rays: memoirs by Röntgen, Stokes, and J. J. Thomson.* Harper's scientific memoirs. Harper & brothers, 1899.

3. E. Levine. *Röntgen and His Rays: Fifty Years Afterwards : Inaugural Lecture.* Witwatersrand University Press, 1974.

4. O. Glasser. *Wilhelm Conrad Röntgen and the Early History of the Roentgen Rays.* Norman radiology series. Norman Pub., 1993.

5. K. Iniewski. *Medical Imaging: Principles, Detectors, and Electronics.* Wiley, 2009.

6. E. Whaites. *Essentials of Dental Radiography and Radiology.* Elsevier Health Sciences UK, 2006.

7. R.L. Webber and U.E. Ruttimann. Dental imaging. In *Image Management and Communication in Patient Care, 1989. Implementation and Impact., First International Conference on*, pages 276 –281, jun 1989.

8. M. Rantala, S. Vanska, S. Jarvenpaa, M. Kalke, M. Lassas, J. Moberg, and S. Siltanen. Wavelet-based reconstruction for limited-angle x-ray tomography. *Medical Imaging, IEEE Transactions on*, 25(2):210 –217, feb. 2006.

9. K. Bliznakova, Z. Bliznakov, and I. Buliev. Comparison of algorithms for out-of-plane artifacts removal in digital tomosynthesis reconstructions. *Comput Methods Programs Biomed*, Nov 2011.

10. J. T. Dobbins and D. J. Godfrey. Digital x-ray tomosynthesis: current state of the art and clinical potential. *Phys Med Biol*, 48(19):65–106, Oct 2003.

11. C. Badea, Z. Kolitsi, and N. Pallikarakis. Image quality in extended arc filtered digital tomosynthesis. *Acta Radiol*, 42(2):244–248, Mar 2001.

12. J. Duryea, J. T. Dobbins, and J. A. Lynch. Digital tomosynthesis of hand joints for arthritis assessment. *Med Phys*, 30(3):325–333, Mar 2003.

13. M. A. Speidel, B. P. Wilfley, A. Hsu, and D. Hristov. Feasibility of low-dose single-view 3D fiducial tracking concurrent with external beam delivery. *Med Phys*, 39(4):2163–2169, Apr 2012.

14. X. Qian, A. Tucker, E. Gidcumb, J. Shan, G. Yang, X. Calderon-Colon, S. Sultana, J. Lu, O. Zhou, D. Spronk, F. Sprenger, Y. Zhang, D. Kennedy, T. Farbizio, and Z. Jing. High resolution stationary digital breast tomosynthesis using distributed carbon nanotube x-ray source array. *Med Phys*, 39(4):2090–2099, Apr 2012.

15. D. G. Grant. Tomosynthesis: a three-dimensional radiographic imaging technique. *IEEE Trans Biomed Eng*, 19(1):20–28, Jan 1972.

16. S. K. Ng, Y. Lyatskaya, D. Stsepankou, J. Hesser, J. R. Bellon, J. S. Wong, and P. Zygmanski. Automation of clip localization in Digital Tomosynthesis for setup of breast cancer patients. *Phys Med*, Dec 2011.

17. T. Gomi, M. Nakajima, H. Fujiwara, T. Takeda, K. Saito, T. Umeda, and K. Sakaguchi. Comparison between chest digital tomosynthesis and CT to detect artificial pulmonary nodules for screening: a phantom study. *Br J Radiol*, Mar 2012.

18. Guenter Lauritsch and Wolfgang H. Haerer. Theoretical framework for filtered back projection in tomosynthesis. volume 3338, pages 1127–1137. SPIE, 1998.

19. Z. Kolitsi, G. Panayiotakis, V. Anastassopoulos, A. Scodras, and N. Pallikarakis. A multiple projection method for digital tomosynthesis. *Med Phys*, 19(4):1045–1050, 1992.

20. Z. Kolitsi, G. Panayiotakis, and N. Pallikarakis. A method for selective removal of out-of-plane structures in digital tomosynthesis. *Med Phys*, 20(1):47–50, 1993.

21. Zhou Wang, A.C. Bovik, H.R. Sheikh, and E.P. Simoncelli. Image quality assessment: from error visibility to structural similarity. *Image Processing, IEEE Transactions on*, 13(4):600 –612, april 2004.